DEVELOPMENT AND OPERATION OF
A HEMI-ELLIPSOIDAL MIRROR INFRARED REFLECTOMETER
FROM 2 TO 34 μm

VON KÁRMÁN GAS DYNAMICS FACILITY
ARNOLD ENGINEERING DEVELOPMENT CENTER
AIR FORCE SYSTEMS COMMAND
ARNOLD AIR FORCE STATION, TENNESSEE 37389

July 1975

Final Report for Period July 1, 1973 — June 30, 1974

Prepared for

DIRECTORATE OF TECHNOLOGY
ARNOLD ENGINEERING DEVELOPMENT CENTER
ARNOLD AIR FORCE STATION, TENNESSEE 37389

This report has been reviewed by the Information Office (OI) and is releasable to the National Technical Information Service (NTIS). At NTIS, it will be available to the general public, including foreign nations.
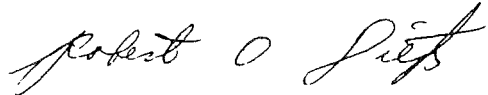
APPROVAL STATEMENT

This technical report has been reviewed and is approved for publication.

FOR THE COMMANDER

MELVIN L. GUIOU
Captain, USAF
Research & Development
   Division
Directorate of Technology

ROBERT O. DIETZ
Director of Technology

REPORT DOCUMENTATION PAGE		READ INSTRUCTIONS BEFORE COMPLETING FORM
1. REPORT NUMBER AEDC-TR-75-64	2. GOVT ACCESSION NO.	3. RECIPIENT'S CATALOG NUMBER
4. TITLE (and Subtitle) DEVELOPMENT AND OPERATION OF A HEMI-ELLIPSOIDAL MIRROR INFRARED REFLECTOMETER FROM 2 TO 34 μm		5. TYPE OF REPORT & PERIOD COVERED Final Report, July 1, 1973 to June 30, 1974
		6. PERFORMING ORG. REPORT NUMBER
7. AUTHOR(s) B. E. Wood, J. G. Pipes, A. M. Smith, and J. A. Roux, ARO, Inc.		8. CONTRACT OR GRANT NUMBER(s)
9. PERFORMING ORGANIZATION NAME AND ADDRESS Arnold Engineering Development Center (DY) Arnold Air Force Station, TN 37389		10. PROGRAM ELEMENT, PROJECT, TASK AREA & WORK UNIT NUMBERS Program Element 65802F
11. CONTROLLING OFFICE NAME AND ADDRESS Arnold Engineering Development Center (DYFS), Arnold Air Force Station, TN 37389		12. REPORT DATE July 1975
		13. NUMBER OF PAGES 52
14. MONITORING AGENCY NAME & ADDRESS(if different from Controlling Office)		15. SECURITY CLASS. (of this report) UNCLASSIFIED
		15a. DECLASSIFICATION/DOWNGRADING SCHEDULE N/A

16. DISTRIBUTION STATEMENT (of this Report)

Approved for public release; distribution unlimited.

17. DISTRIBUTION STATEMENT (of the abstract entered in Block 20, if different from Report)

18. SUPPLEMENTARY NOTES

Available in DDC.

19. KEY WORDS (Continue on reverse side if necessary and identify by block number)

reflectometers
infrared radiation
infrared spectrum
infrared equipment

ellipsoids
ray tracing
reflection
coatings

20. ABSTRACT (Continue on reverse side if necessary and identify by block number)
The development and testing of an infrared hemi-ellipsoidal mirror reflectometer (HEMR) operational over a wavelength interval from 2 to 34 μm is described. This optical system measures the hemispherical-directional reflectance of room temperature samples relative to a specular, gold-coated surface. It is shown theoretically that for infinitesimal source and sample areas the HEMR measures the hemispherical-directional reflectance. Further,

DD FORM 1473 1 JAN 73   EDITION OF 1 NOV 65 IS OBSOLETE

20, Continued

for a source and sample area commensurate with energy requirements, it is shown experimentally that the HEMR is functional, with very tolerable errors. Several associated problem areas investigated are described in detail. Finally, the hemispherical-directional reflectance of test samples (e.g., black paints, gold diffuser, sulfur, cesium iodide, and others) is presented for wavelengths from 2 to 34 μm. The HEMR has proven to be a very practical reflectometer with direct applications associated with test projects at AEDC.

AFSC
Arnold AFS Tenn

PREFACE

CONTENTS

ILLUSTRATIONS

TABLE

1.0 INTRODUCTION

Reflectometers are categorized by various factors. Among these are (1) whether they are spectral or all-wavelength (polychromatic), (2) whether they provide directional or hemispherical sample irradiation, (3) whether they use relative or absolute techniques of reflectance measurement, and (4) whether they provide specular or hemispherical collection of reflected radiation. For the most part these reflectance measurements are carried out in (1) integrating spheres, (2) heated cavities, (3) paraboloidal mirrors, and (4) hemispherical or ellipsoidal mirrors. Each system has its distinct characteristics, advantages and disadvantages. Integrating spheres are the most widely used for measurements in the solar wavelength range (0.3 to 2.5 μm) although some have been extended to 12 μm using a sodium chloride coating (Refs. 1 and 2). Heated cavity reflectometers have been commonly used in the 2- to 15-μm range. For wavelengths longer than about 15 μm, either specular reflectance measurements are made or the measurements are carried out in some type of 2π steradian mirror such as paraboloidal, hemi-ellipsoidal or hemispherical mirrors. Reflectance measurements out to 100 μm have been reported in Refs. 3 and 4 using these types of systems. This report discusses the development and operation of a hemi-ellipsoidal mirror reflectometer (HEMR) which presently has a reflectance measurement capability for wavelengths in the 2- to 34-μm range. This wavelength range capability makes the instrument extremely useful for support of infrared sensor tests in AEDC Aerospace Chamber 7V since the reflectance and transmission of components such as mirrors, filters, windows, etc. can be measured. In addition, the application of the HEMR to other tests at AEDC is discussed; applications include the determination of aerodynamic heating temperatures using the infrared camera in AEDC wind tunnels and thermal balance testing in AEDC Aerospace Chamber 12V.

2.0 DESCRIPTION

A schematic of the ellipsoidal mirror is shown in Fig. 1. The mirror was designed to have a semimajor axis of b = 6.0 in. and semiminor axes of a = 5.916 in. This yields an ellipse eccentricity of e = 0.1667 and a d = 2-in. separation of the foci. A small separation of the two foci is desirable since the magnification and aberration decrease as the foci separation is decreased (Ref. 5). The mathematical equation of the ellipsoid is given by

$$\frac{x^2 + z^2}{a^2} + \frac{y^2}{b^2} = \frac{x^2 + z^2}{(5.916)^2} + \frac{y^2}{(6.0)^2} = 1 \tag{1}$$

where y is the coordinate direction along the major axis and x and z are the coordinate directions along the minor axes. This is mathematically a prolate spheroid which can be generated as a surface of revolution by revolving the ellipse $(z^2/a^2) + (y^2/b^2) = 1$ about the y axis (major axis). The ellipsoid has the property that radiation emitted in any direction from a source placed at one foci, F_1, will be reflected by the mirror and focused at the conjugate foci, F_2. The experimental arrangement for the reflectometer is shown in Fig. 2. Here a blackbody source is placed at one foci (F_1) and the test sample at the other (F_2); this provides a means of irradiating the sample hemispherically and, as will be shown later, diffusely. Since the test sample is thus irradiated uniformly from all directions, and reflected radiation is collected in a given direction, the hemispherical-directional reflectance is the property measured.
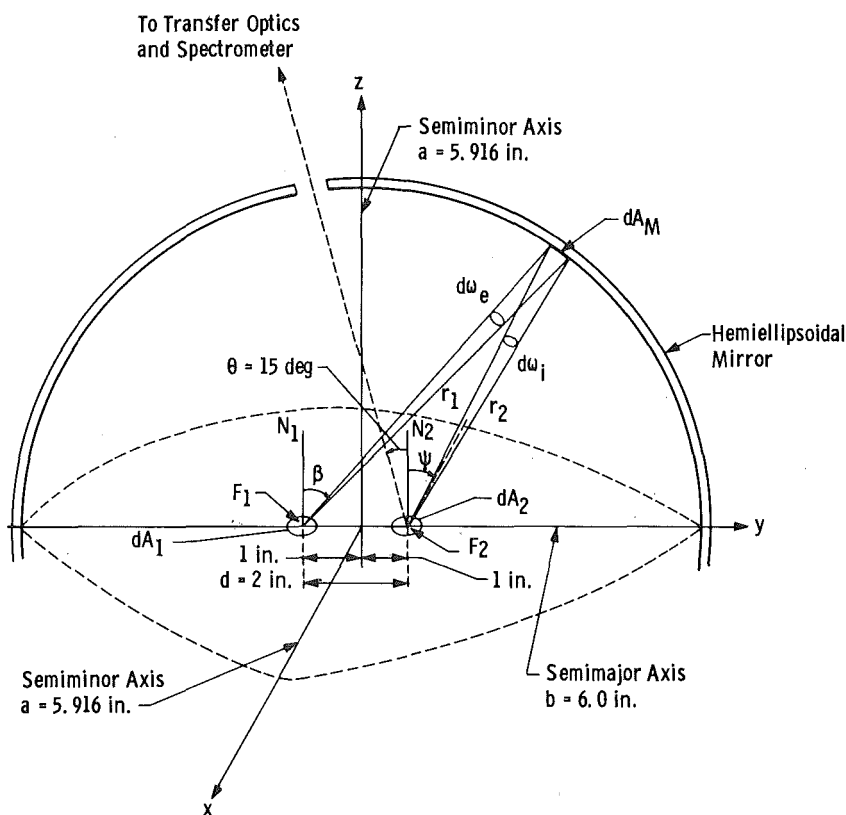
Figure 1. Schematic of hemi-ellipsoidal mirror reflectometer and coordinate system.
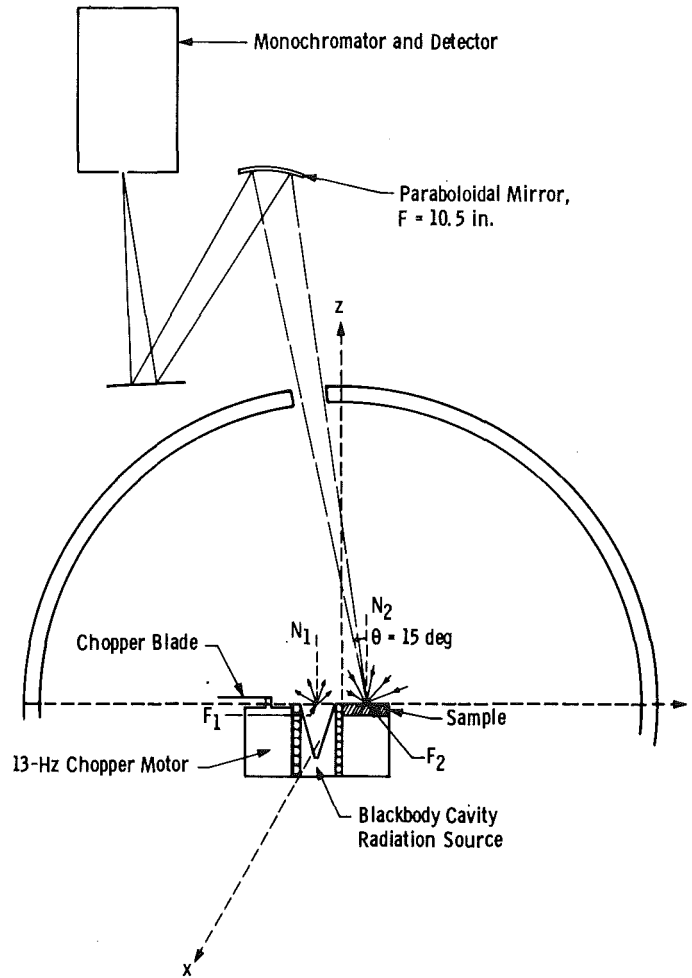
Figure 2. Experimental arrangement of reflectometer.

Figure 3 shows the source, sample, and ellipsoid coordinate systems and their geometrical relationship. Assume first of all that the blackbody has a spectral emissivity of 1.0 and that the emitted spectral intensity $I_b(\beta, \gamma)$ through solid angle $d\omega_e$ is uniform regardless of direction β, γ (β is the polar angle measured relative to the source normal N_1, and γ is the azimuthal angle measured relative to the $+y$ axis. The monochromatic intensity $I_i(\psi, \zeta)$ $(w/cm^2-sr-\mu m)$ incident at the sample foci is given by

$$I_i(\psi,\zeta) = \rho_M I_b(\beta,\gamma) \qquad (2)$$

where ρ_M is the spectral mirror reflectance, ψ is the polar angle of incidence as measured from N_2, and ζ is the azimuthal angle measured

from the $+y$ axis (see Fig. 3). The hemispherical-directional reflectance of a surface located at the sample foci is defined as

$$\rho_{hd}(\theta,\phi) = \frac{1}{\pi} \int_{2\pi} \rho_{bd}(\psi,\zeta;\theta,\phi) \cos\psi \, d\omega_i \tag{3}$$

where $d\omega_i$ is the incidence solid angle and $\rho_{bd}(\psi, \zeta; \theta, \phi)$, the bidirectional reflectance, is defined (Ref. 6) as

$$\rho_{bd}(\psi,\zeta;\theta,\phi) = \frac{\pi \, dI_R(\theta,\phi)}{I_i(\psi,\zeta) \cos\psi \, d\omega_i} \tag{4}$$

where θ is the polar reflection angle measured from N_2 and ϕ is the azimuthal reflection angle (see Fig. 3). In Eq. (4) $dI_R(\theta, \phi)$ is the differential intensity reflected in the θ, ϕ direction because of the surface's being irradiated from the direction ψ, ζ with intensity $I_i(\psi, \zeta)$ through the solid angle $d\omega_i$. The intensity of the radiation reflected in the θ, ϕ direction because of the test surface's being irradiated from all ψ, ζ directions then is found from

$$I_R(\theta,\phi) = \int_{2\pi} dI_R(\theta,\phi) = \frac{1}{\pi} \int_{2\pi} \rho_{bd}(\psi,\zeta;\theta,\phi) I_i(\psi,\zeta) \cos\psi \, d\omega_i \tag{5}$$

Since $I_i(\psi, \zeta)$ is a constant for diffuse incidence, it can be taken outside the integral, and by use of Eq. (3), one can reduce Eq. (5) to

$$I_R(\theta,\phi) = I_i(\psi,\zeta)\rho_{hd}(\theta,\phi) \tag{6}$$

therefore,

$$I_i(\psi,\zeta) = \text{constant}$$

Thus the intensity reflected is equivalent to the incident intensity decreased by the sample reflectance $\rho_{hd}(\theta, \phi)$. This is true for all surfaces regardless of the bidirectional reflectance distribution function. This means that diffuse surfaces can be measured as simply as specular surfaces.

The power, $d\dot{q}_S$, reflected from a sample surface of unknown reflectance per unit surface area in the direction θ, ϕ and contained in the reflection solid angle $d\omega_R$ can be expressed as

$$d\dot{q}_S = I_R(\theta,\phi) \cos\theta \, d\omega_R = \rho_{hd,S}(\theta,\phi) I_i(\psi,\zeta) \cos\theta \, d\omega_R \tag{7}$$

Similarly, the power reflected from a reference surface whose reflectance is known would be

$$d\dot{q}_{Ref} = \rho_{hd,Ref}(\theta,\phi)I_i(\psi,\zeta) \cos\theta \, d\omega_R \qquad (8)$$

The detector outputs for the two cases are directly related to the reflected power. By ratioing Eqs. (7) and (8), then

$$\frac{\rho_{hd,S}(\theta,\phi)}{\rho_{hd,Ref}(\theta,\phi)} = \frac{d\dot{q}_S}{d\dot{q}_{Ref}} = \frac{K'd\dot{q}_S}{K'd\dot{q}_{Ref}} = \frac{B_S}{B_{Ref}} \qquad (9)$$

where B_S and B_{Ref} are the two detector outputs observed for the test surface and reference surface, respectively. The detector output is proportional to the reflected power through the detection constant K', which depends on the type of detector used as well as the characteristics of the transfer optics. Equation (9) presents a convenient method for determining the hemispherical-directional reflectance of an unknown surface, especially if the reference surface has a reflectance value near unity (such as a gold mirror for infrared wavelengths).
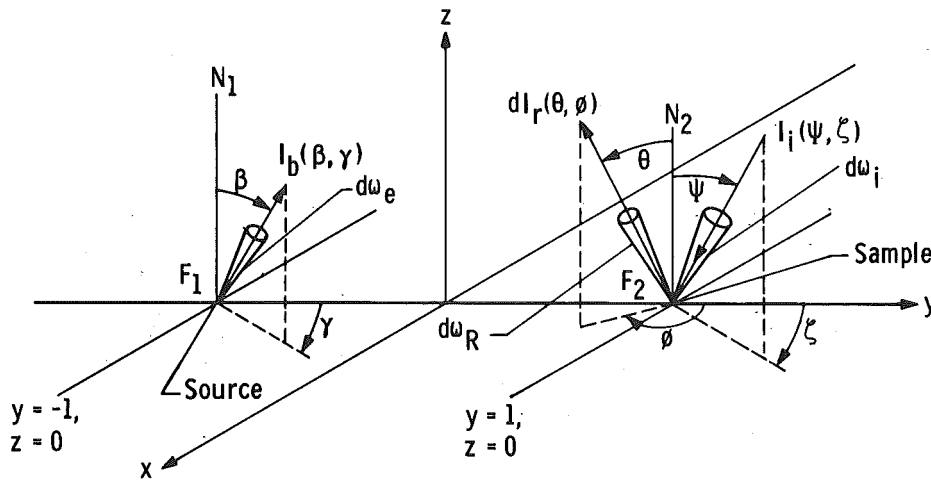
Figure 3. Source, sample, and ellipsoid coordinate systems, and their geometrical relationship.

In order to realize in practice a ρ_{hd} measurement in the HEMR as determined through the use of Eq. (9), it is necessary that (1) the blackbody have a spectral directional emissivity of near unity over 2π sr and (2) the aberrations introduced by the hemiellipsoidal mirror be negligible so that the test surface is uniformly irradiated. These problem areas were systematically examined for possible error sources and to define the best possible design of radiation source, chopper, and sample.

It should be mentioned that the approach of placing a blackbody at one foci and the test surface at the conjugate foci is only one of three or four approaches considered. The other most promising approach was that of operating the HEMR in the directional-hemispherical mode. That is, the test surface was irradiated from a given direction and the hemispherically reflected radiation was refocused by the ellipsoidal mirror on a detector located at the conjugate foci. This technique would have the major advantage that only a small heat load would be placed on the sample since monochromatic radiation would be incident rather than of all wavelengths. However, the difficulty that arose was obtaining a detector which has a uniform (cosine) response to radiation coming in from all directions (hemispherically irradiated) since most flat surfaces have a directional reflectance dependence similar to that given by Fresnel's equations. Adding to the problem was the fact that a relatively large area detector was required, which usually means a thermopile or some type of thermal detector. This approach was attempted, but the directional and spatial nonuniformity of the thermo-pile detector was too great to allow any meaningful measurements. The eventual conclusion reached was that it is much easier to build a diffuse blackbody than it is to obtain a large area detector having a uniform and high sensitivity.

3.0 APPARATUS

The arrangement of the hemi-ellipsoidal mirror and components for the bench tests is shown in the photographs in Figs. 4 and 5. The hemi-ellipsoidal mirror was obtained commercially and was made by molding 3/4-in. Pyrex® into a hemisphere. The outside diameter was essentially that of a hemisphere 13.5 in. in diameter. Grinding and polishing the interior produced the desired configuration and dimensions. The end result was a high quality mirror surface with a semimajor axis of 6 in. and semiminor axes of 5.916 in. The mirror coating was vacuum-deposited aluminum, which has a reflectivity of 97 to 99 percent in the 2- to 35-μ range. A hole 1.50 in. in diameter was cut in the mirror to pass the radiation reflected from the opposite foci (see Fig. 1). The location of the hole was such that the center corresponded to reflection angles of θ = 15 deg and ϕ = 180 deg.

A commercially built blackbody was used for the radiation source. It was constructed of oxygen-free copper and was machined to form a blunt cone. Metal-sheathed electric heating elements were wound around

12
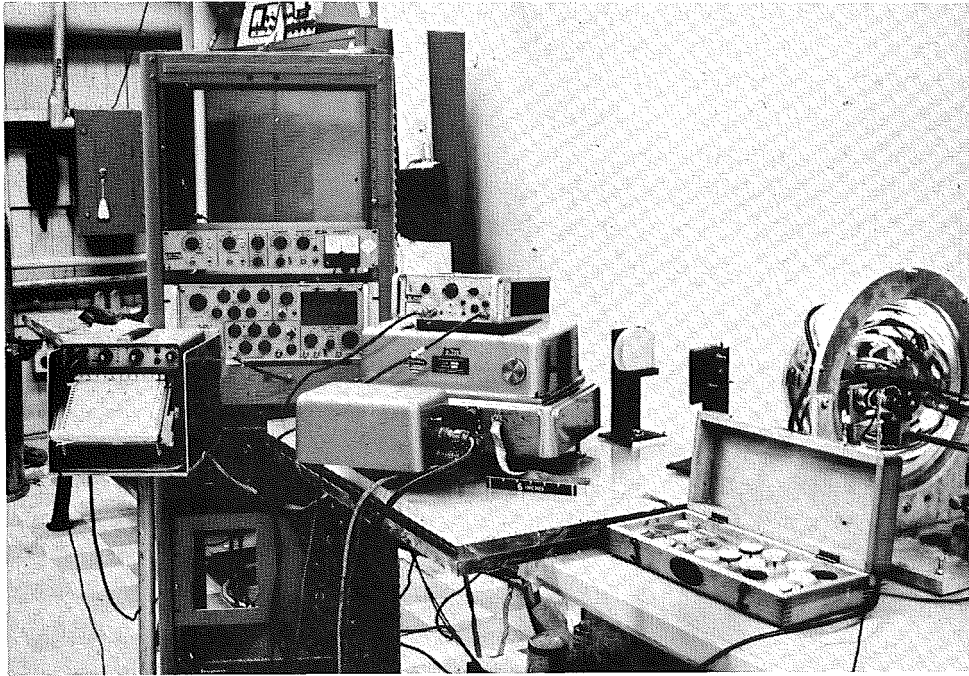
Figure 4. Hemi-ellipsoidal mirror reflectometer.
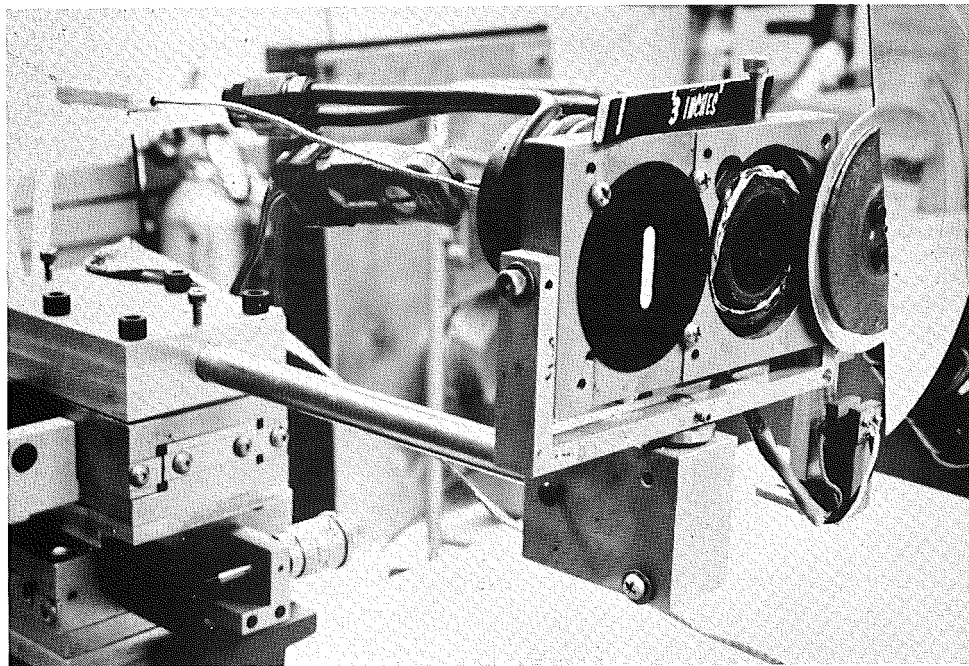
Figure 5. Sample and blackbody with chopper attached to yoke.

the exterior and brazed to the copper surface with a gold-copper alloy.
The interior of the cone was plasma-sprayed with stainless steel, which
oxidizes at around 900°F to form a high emissive coating. Normal oper-
ating temperature of the blackbody was between 800 and 900°F. The
blackbody cavity opening was 1 in. in diameter, and the cavity depth
was 1.375 in., yielding an L/R ratio of 2.75 where L is the depth and R
is the cavity radius. Normal operation required a power of about 60 w,
and after the blackbody temperature reached equilibrium it was stable
within ±1/2°F.

Radiation emitted from the blackbody was modulated at a frequency
of 13 Hz by locating the polished aluminum chopper blade as close as
possible to the cavity exit (see Fig. 5). Using a chopped signal elimi-
nated the troublesome self-emission error that is present in heated-
cavity-type reflectometers. The chopper, blackbody, and sample
holder were all mounted on a yoke arrangement that was mounted on an
X-Y micropositioner (Figs. 4 and 5). The yoke plus the X-Y translator
provided 6 deg of freedom to allow alignment of the plane containing the
source and samples with the equatorial plane of the ellipsoidal mirror.
The blackbody and sample holder were mounted with a 2-in. separation
from center to center, which corresponded to the separation of the
mirror foci. Radiation reflected from the sample or reference surface,
passed through the hole in the HEM, and was collected by an off-axis
paraboloidal mirror and focused on the entrance slit of a single-pass
Perkin-Elmer® monochromator. Depending on the wavelength range of
interest, either a KBr prism (2 to 25 μm) or a CsBr prism (14 to 34 μm)
was used as the monochromator dispersing element. A Reeder® thermo-
couple was the detector. From the detector the signal was amplified
with a phase lock amplifier and displayed on a strip chart recorder.
The resolution for the single-pass monochromator with the KBr prism
was determined for typical slit widths used in making reflectance mea-
surements. These values were calculated from the relation

$$\Delta\lambda = \Delta\lambda_p + \Delta\lambda_{(0.1)} \times \text{slit width}/0.1$$

The values for $\Delta\lambda_p$ and $\Delta\lambda_{(0.1)}$ were furnished by the Perkin-Elmer
Corporation. Typical $\Delta\lambda$ values and slit widths used were as follows:
at λ = 3 μm, $\Delta\lambda$ = 0.05 μm for 0.04-mm slits; at λ = 5 μm, $\Delta\lambda$ = 0.076
μm for 0.04-mm slits; at λ = 10 μm, $\Delta\lambda$ = 0.086 μm for 0.1-mm slits;
at λ = 15 μm, $\Delta\lambda$ = 0.096 μm for 0.2-mm slits; and at λ = 25 μm,
$\Delta\lambda$ = 0.119 μm for 0.5-mm slits.

Alignment of the sample, blackbody, ellipsoidal mirror, transfer optics, and monochromator was accomplished in the following way. Since the sample and blackbody were rigidly mounted on the X-Y translator 2 in. apart, the problem was to locate them at the two mirror foci. The ellipsoid major and minor axes in the equatorial plane were given by the manufacturer, so the blackbody and sample were aligned with these axes. Determination of the location in the z direction (into the mirror) was accomplished by temporarily replacing the blackbody with a tiny pinhole light positioned at the blackbody center, and placing a white card at the sample location. The entire yoke assembly was then moved in and out of the HEM until the best focus of the pinhole light was obtained at the conjugate foci. This in effect spatially located the mirror foci. The next problem was to align the monochromator and transfer optics with the HEM. This was accomplished by passing the mercury green line (λ = 0.5461 μm) in the reverse direction through the monochromator and transfer optics and bringing it to focus on the white card at the sample location within the HEM. At this time it was also determined that the reflected light from the card was in turn imaged at the center of the blackbody. Final alignment consisted of peaking the detector output by minor adjustments of the monochromator position.

4.0 PERFORMANCE REQUIREMENTS FOR MEASURING THE HEMISPHERICAL-DIRECTIONAL REFLECTANCE

As shown in Eq. (9), the hemi-ellipsoidal reflectometer will be used to measure the hemispherical-directional reflectance. Physically the hemispherical-directional reflectance, ρ_{hd}, is defined as the ratio of the intensity reflected from an infinitesimal area dA, collected in a specific angular direction, to the incident intensity which is hemispherically and diffusely distributed. The hemi-ellipsoidal infrared reflectometer described in this report was designed for the purpose of measuring ρ_{hd} in a reflection direction θ = 15 deg, ϕ = 180 deg. In order to facilitate the measurement of ρ_{hd} of a sample material, the infrared reflectometer must satisfy two basic requirements: (1) the source must be a diffuse emitter of radiation, and (2) the sample must be diffusely irradiated with constant intensity. To show that these two system criteria were fulfilled, the blackbody source intensity and the irradiation of the sample location were studied in detail, both analytically and experimentally.

4.1 BLACKBODY RADIATION DISTRIBUTION MEASUREMENTS

As mentioned previously, the first requirement for the successful operation of the HEMR is that the radiation source be diffuse; that is, the emitted intensity (w/cm^2-sr-μm) should be constant with the view angle β (or the emitted power distribution should be a cosine curve). The emitted intensity distribution of the blackbody source was measured using the apparatus shown in Fig. 6. The blackbody was mounted on a rotary table with the facial plane of the blackbody coincident with the rotary table center of rotation. Radiation emitted by the blackbody into a solid angle of approximately 0.058 sr was chopped at 13 Hz and focused by a paraboloidal mirror on a pyroelectric detector after passing through a 19.1 to 22.5-μm bandpass filter. The results are presented in Fig. 7, where the normalized intensity is plotted versus view angle β. Positive values of β correspond to $\gamma = 0$ and negative β values correspond to $\gamma = 180$ deg. As seen, the intensity is reasonably constant except at the two extremes (i.e., for $\beta > 80$ deg or $\beta < -80$ deg), where the intensity falls rapidly to zero. The reason for
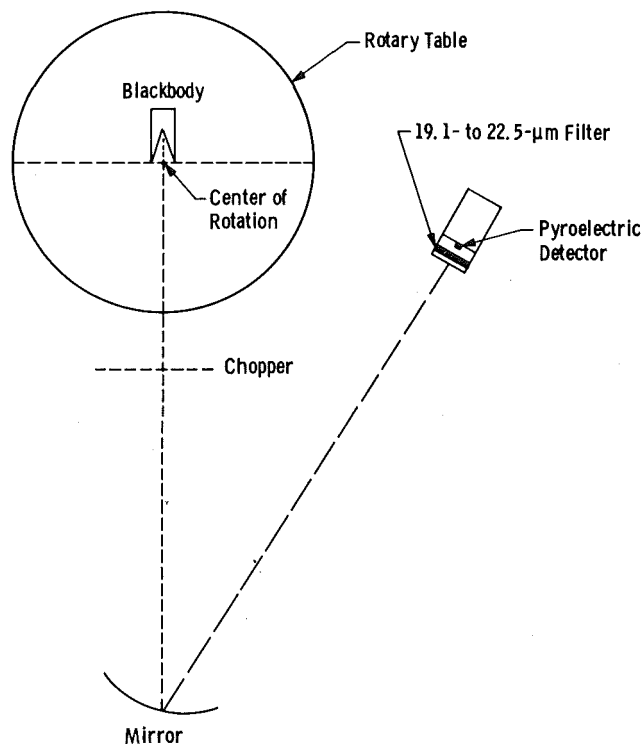
Figure 6. Apparatus for blackbody radiation distribution measurements.

this is that at these higher angles, the detector is directly viewing the cavity wall near the exit, effectively reducing the emissivity since the wall near the exit would not appear as "black" as the central portion of the cavity. Figure 8 shows a plot of the same data as are shown in Fig. 6, but here the normalized power emitted by the blackbody rather than intensity is presented as a function of β. This curve shows that the blackbody is essentially diffuse over that portion of the cone in which nearly all of the energy is concentrated, $\beta \le 75$ deg. The normalized intensity distribution of the blackbody across the exit was measured by scanning across the blackbody with the detector looking normal to the blackbody at all times. Such a scan is shown in Fig. 9. Again, the distribution is relatively constant over the central core of the cavity but falls off near the edges. Data similar to those shown in Figs. 7, 8, and 9 were obtained for the blackbody rotated about its longitudinal axis 90, 180, and 270 deg from the original orientation. In all cases the results were the same as those presented in Figs. 7, 8, and 9. Since the only portion of the blackbody distribution curve that departs from the cosine curve is at the extremely high angles, very little if any error will be introduced. The worst case condition would be in measuring a highly diffuse reflector in the infrared. This would result in a reflectance reading that could be slightly low. Fortunately, most surfaces in the infrared tend
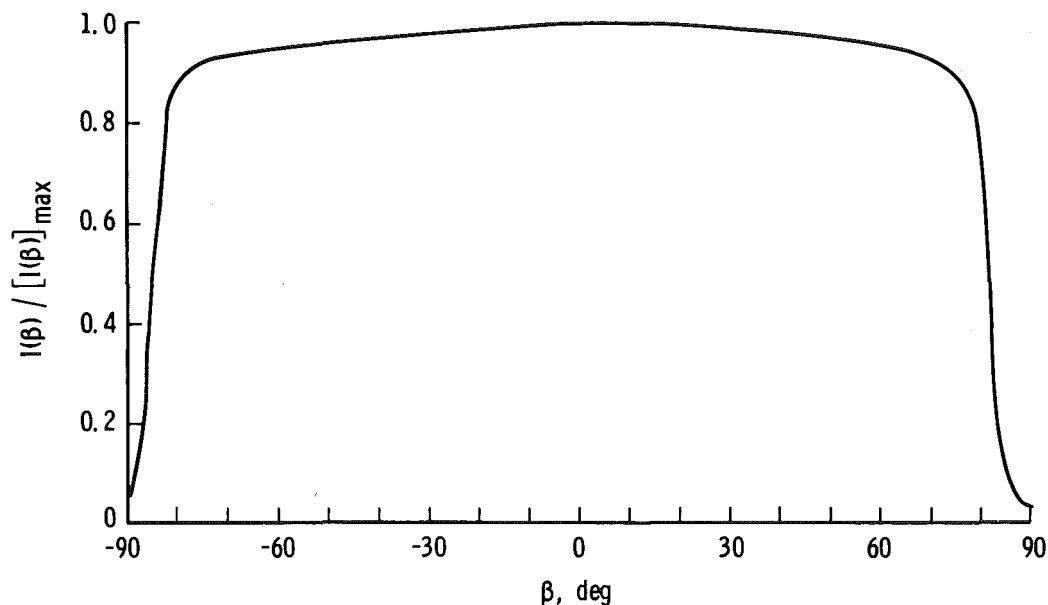
Figure 7. Blackbody intensity distribution measurements, 19.1 μm $< \lambda <$ 22.5 μm.

to become more specular in going to longer wavelengths and as a result the reflected energy is more or less concentrated about the specular direction rather than being diffusely reflected. This characteristic then diminishes the role of the radiation emitted by the blackbody at the higher angles and reduces the error involved. It is believed that this blackbody comes as close to being a near-perfect diffuse emitter as is practically possible.
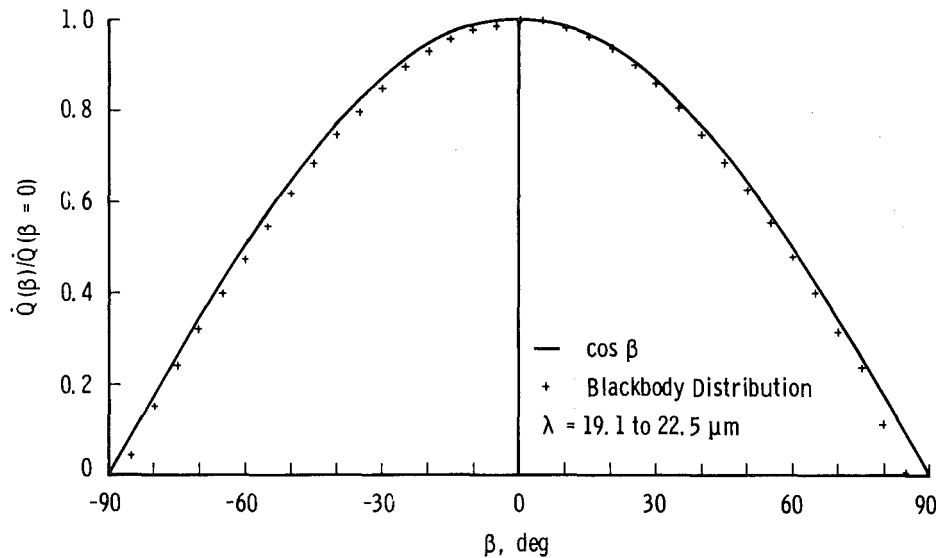
Figure 8. Emitted power distribution of blackbody source, 19.1 μm $<$ λ $<$ 22.5 μm.
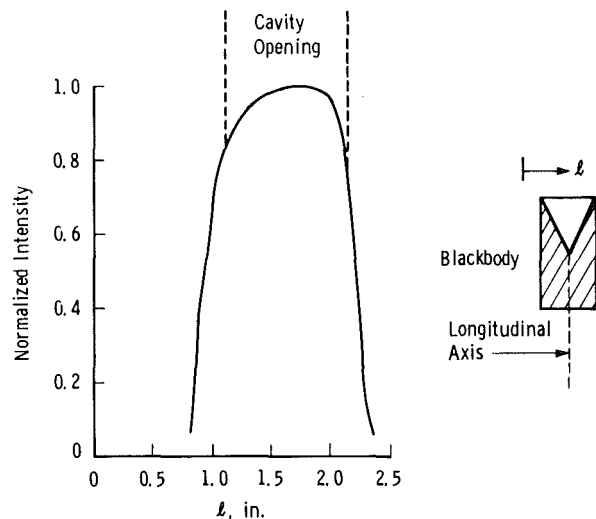
Figure 9. Intensity scan across blackbody, 19.1 μm $<$ λ $<$ 22.5 μm.

4.2 FOCUSING PROPERTIES OF THE HEMI-ELLIPSOIDAL MIRROR

It has been shown that the blackbody source does approach being an ideal diffuse emitter of radiation; it now remains to show that the sample will be uniformly irradiated with a constant intensity (diffusely irradiated). This requires that the hemi-ellipsoidal mirror collect and focus the diffusely emitted radiation from the source in such a manner that the sample is diffusely irradiated at the sample foci. The reflection, or focusing, characteristics of the hemiellipsoidal mirror will be determined and compared using essentially three different approaches: (a) Analytical determination of the focusing characteristics for ideal infinitesimal source and sample areas, (b) use of a rigorous ray-tracing technique, and (c) comparison of experimental data with analytical requirements.

4.2.1 Ideal Infinitesimal Source and Sample Areas

In determining whether the sample is diffusely irradiated for ideal infinitesimal areas one must derive an expression for the intensity incident upon a small differential area element, dA_2, centered at the sample foci which is emitted from a differential area element dA_1 centered at the source (blackbody) foci as shown in Fig. 1. The mirror is assumed to have a constant reflectance given by ρ_M. The power emitted from dA_1 and incident upon dA_M (a differential area element of the hemi-ellipsoidal mirror) is given by

$$d\dot{Q}_M = \frac{I_b \cos \beta \, dA_1 \cos \alpha \, dA_M}{r_1^2} \tag{10}$$

where I_b is the diffuse monochromatic intensity emitted from dA_1 (source) and r_1 is the distance from dA_1 to dA_M (as shown in Fig. 1). The angle of incidence at dA_M is equal to the reflection angle α because the facet of the mirror dA_M acts as a plane specular reflector. The power reflected from dA_M and incident on dA_2 is given by

$$d\dot{Q}_2 = \frac{\rho_M I_b \cos \beta \, dA_1 \cos \alpha \, dA_M}{r_1^2} \tag{11}$$

This power is contained in the solid angle $d\omega_i$. The definition of the intensity incident upon dA_2 is given by

$$I_i = \frac{d\dot{Q}_2}{d\omega_i \cos \psi \, dA_2} \tag{12}$$

19

with

$$d\omega_i = \frac{dA_M \cos \alpha}{r_2^2} \qquad (13)$$

If one substitutes $d\omega_i$ from Eq. (13) and $d\dot{Q}_2$ from Eq. (11) into Eq. (12), the intensity incident upon dA_2 then becomes

$$I_i = \rho_M I_b \left(\frac{\cos \beta}{\cos \psi}\right)\left(\frac{dA_1}{dA_2}\right)\left(\frac{r_2}{r_1}\right)^2 \qquad (14)$$

Now if the intensity at dA_2 is to be a constant (diffuse) for all values of β, then I_i must be a constant. Since ρ_M and I_b are constants, then it must be shown that

$$\left(\frac{\cos \beta}{\cos \psi}\right)\left(\frac{dA_1}{dA_2}\right)\left(\frac{r_2}{r_1}\right)^2 = \text{constant} \qquad (15)$$

Because each mirror element dA_M can be treated as an infinitesimal flat mirror, then by the fundamental law of reflection from plane specular surfaces it is known that the incident solid angle and the solid angle of reflection are equal, hence

$$\frac{dA_1 \cos \beta}{r_1^2} = d\omega_1 = d\omega_2 = \frac{dA_2 \cos \psi}{r_2^2} \qquad (16)$$

where $d\omega_1$ is the solid angle subtended by dA_1 with respect to dA_M, and $d\omega_2$ is the solid angle subtended by dA_2 with respect to dA_M. Rearranging Eq. (16) yields

$$\frac{dA_1 \cos \beta}{dA_2 \cos \psi} \left(\frac{r_2}{r_1}\right)^2 = 1 \qquad (17)$$

and Eq. (14) becomes

$$I_i = \rho_M I_b = \text{constant} \qquad (18)$$

This proves that for a diffuse source the sample will be diffusely irradiated, thus fulfilling one of the requirements necessary for measuring ρ_{hd}. Hence, for each β there results an r_1, r_2, and ψ which satisfies Eq. (17). Furthermore, Eq. (17) can be used to determine the area magnification, $M(\beta, \gamma)$, resulting from any arbitrary mirror element dA_M; i.e.,

$$M(\beta,\gamma) \equiv \frac{dA_2}{dA_1} = \left(\frac{\cos \beta}{\cos \psi}\right)\left(\frac{r_2}{r_1}\right)^2 \tag{19}$$

This simple derivation shows that the hemi-ellipsoidal mirror must magnify or demagnify according to Eq. (19) if the sample is to be truly diffusely irradiated. To evaluate Eq. (19) analytically it is necessary to determine ψ, r_1, and r_2 as a function of β and the mirror eccentricity e. The derivation which follows will be valid for radiation emitted in the plane formed by the normals to the source and sample and the major axis of the hemi-ellipsoidal mirror. This derivation can also be shown to be valid for other planes passing through the hemi-ellipsoidal major axis, but the derivation is more complex (shown later) and will not serve the purpose of explanation sought here. From Fig. 1 and the law of cosines one may write for γ, $\zeta = 0$ and 180 deg,

$$r_1^2 = r_2^2 + d^2 - 2r_2 d \cos (\pi/2 + \psi) \tag{20}$$

and

$$r_2^2 = r_1^2 + d^2 - 2r_1 d \cos (\pi/2 - \beta) \tag{21}$$

Adding Eqs. (20) and (21) yields

$$r_1 \sin \beta - r_2 \sin \psi = d \tag{22}$$

and subtracting Eq. (20) from Eq. (21) gives

$$\frac{r_1^2 - r_2^2}{d} = r_2 \sin \psi + r_1 \sin \beta \tag{23}$$

From the definition of an ellipse it is known that

$$r_1 + r_2 = 2b \tag{24}$$

and

$$d = 2be \tag{25}$$

Solving Eqs. (22), (23), (24), and (25) yields

$$\sin \psi = \frac{\sin \beta (1 + e^2) - 2e}{1 - 2e \sin \beta + e^2} \tag{26}$$

where from Eq. (22), (23), and (25)

$$r_2 = \frac{2b\,(\sin\beta - e)}{\sin\beta + \sin\psi}$$

(27)

Specifying β, b (or d), and e allows the determination of ψ from
Eq. (26), r_2 from Eq. (27), and then r_1 from Eq. (24). Knowing these
quantities, one can evaluate Eq. (19) for γ, ζ = 0 and 180 deg. Equa-
tion (26) indicates that radiation emitted from dA_1 in direction β will
be incident at dA_2 from direction ψ, and Fig. 10 depicts the results
from Eq. (26)(d = 2 in. and e = 0.1667), showing how these angles
(β and ψ) are related for γ, ζ = 0 and 180 deg. The fact that β and ψ
are not generally equal gives rise to the magnification and demagnifi-
cation characterized by Eq. (19). Positive and negative values of ψ
correspond to ζ values of 0 and 180 deg, respectively.
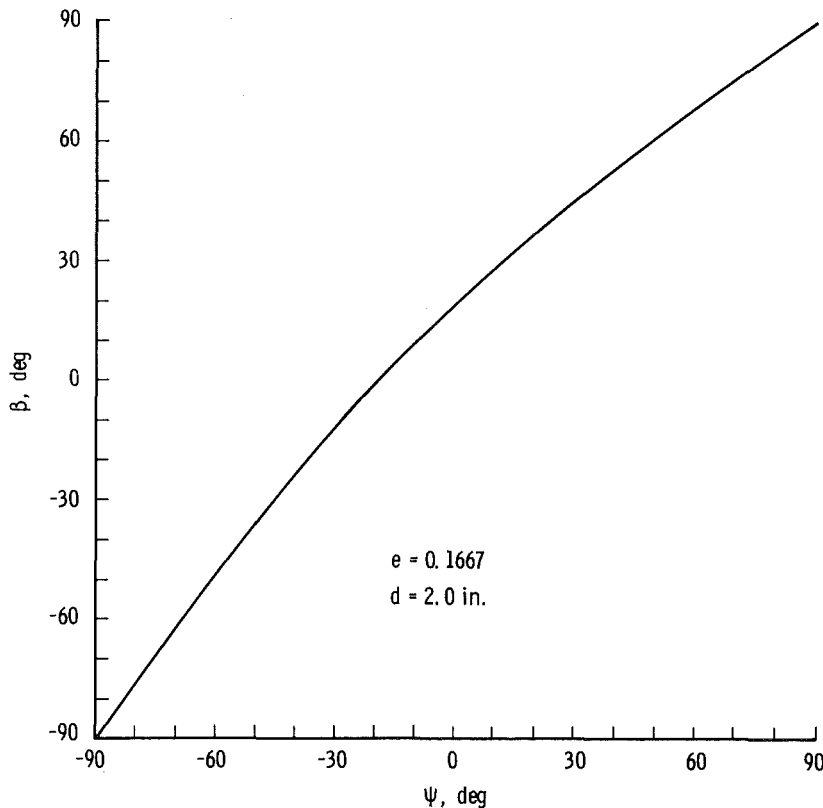
Figure 10. Comparison of blackbody radiance angle β to sample
irradiance angle ψ.

The preceding derivation is valid only for β directions in the plane
formed by the normals to the source and sample and the semimajor axis

(called in-plane derivation). For expressions describing the magnification for other planes (planes not containing the source and sample normals) passing through the semimajor axis (out-of-plane derivation) it is necessary to employ azimuthal angles γ and ζ having values other than 0 and 180 deg. Figure 11 shows the relationship between angles β, γ, ψ, and ζ and the angles needed to perform out-of-plane calculations, β' and ψ'; it is easily seen that

$$\cos \xi = \sin \beta \cos \gamma \tag{28}$$

and

$$\cos \xi' = \sin \psi \cos \zeta \tag{29}$$

with

$$\cos \delta = \cos \beta / \sin \xi = \cos \psi / \sin \xi' \tag{30}$$

where the angle δ is measured in the respective planes normal to the major axis and containing the surface normals N_1 and N_2. Also,

$$\beta' = \pi/2 - \xi \quad , \quad \psi' = \frac{\pi}{2} - \xi' \tag{31}$$

where β' and ψ' are used in place of β and ψ in Eqs. (26) and (27). By specifying β and γ one can determine the angle ξ from Eq. (28). Next, via Eq. (31), β' is computed and then ψ' is evaluated from Eq. (26). From Eqs. (31) and (30), ψ can be determined, and finally, using Eq. (24), one can evaluate Eq. (19).

Thus, via Eq. (19), the magnification characteristics which are required for measuring ρ_{hd} with an ideal hemiellipsoidal reflectometer have been defined. Since the experimental apparatus employs small but finite areas it must be shown that finite areas will approach the same behavior as that required by ideal infinitesimal areas. Also, experimental evidence must be shown that the hemiellipsoidal mirror also exhibits the same magnification characteristics required by Eq. (19).

4.2.2 Finite Area Magnification via Ray Tracing

It has been shown analytically that if the source at F_1 and the sample at F_2 are considered as arbitrary differential area elements dA_1 and dA_2, then the measurement of ρ_{hd} can be realized. It remains to be shown that the aberration introduced by the hemi-ellipsoidal mirror,

$$\cos \xi = \sin \beta \cos \gamma \qquad \cos \xi^* = \sin \psi \cos \zeta$$

$$\cos \delta = \cos \beta \sin \xi \qquad \cos \delta = \cos \psi / \sin \xi^*$$

$$\beta^* = \frac{\pi}{2} - \xi \qquad \psi^* = \frac{\pi}{2} - \xi^*$$
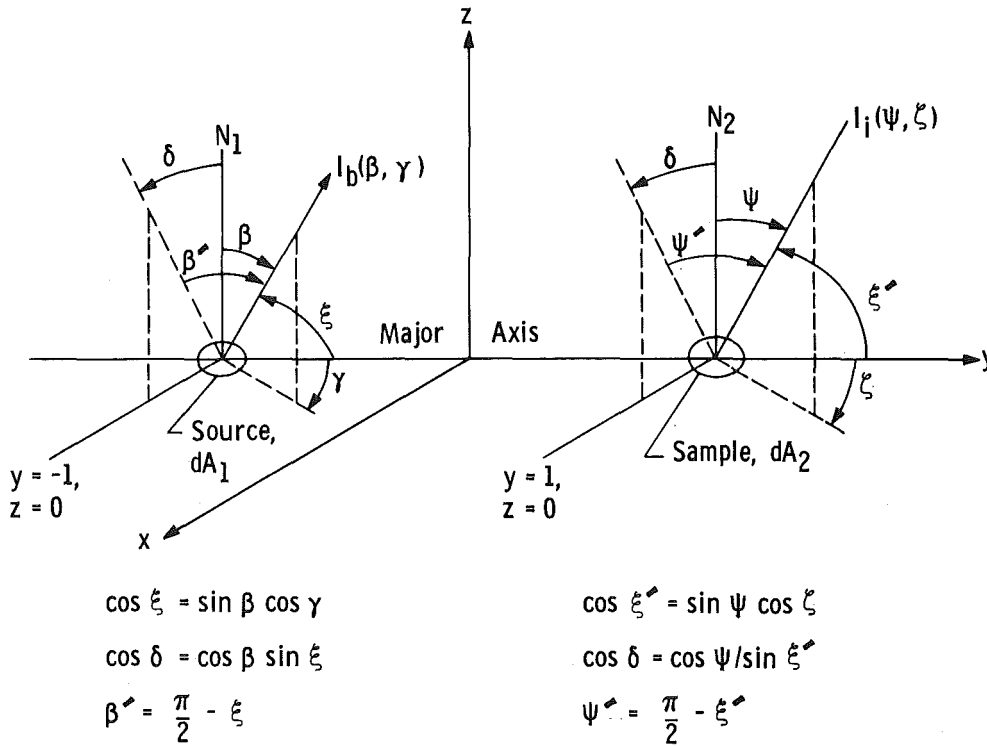
Figure 11. Sketch of geometrical relationships between angles β, λ, ψ, and ζ and angles β' and ψ' necessary to perform out-of-plane calculations of $M(\beta, \gamma)$.

when finite size areas ΔA_1 and ΔA_2 are used, does not jeopardize the reflectometer system; i.e., now the system must be shown to be functional for finite size source and sample areas since in practice the dimensions of the spectrometer entrance slit will dictate these types of areas. The transfer optics are set up for unity magnification. The source of area ΔA_1 was taken to be a 2- x 3-mm rectangular slit (see Fig. 12) which represents the maximum dimensions of the spectrometer entrance slit. Analogous to Eq. (17) and consistent with the notation in Fig. 12, the mathematical requirement for diffuse irradiation of the sample is

$$\frac{r_1^2}{\Delta A_1 \cos \beta} = \frac{r_2^2}{\Delta A_2 \cos \psi} \qquad (32)$$

where ψ is the angle between the normal to the sample and the incident radiation along r_2. As previously required for the infinitesimal areas, this relationship must hold for the diffuse sample irradiation criteria to be obeyed. The values of r_1, r_2, $\cos \beta$, and $\cos \psi$ are readily found
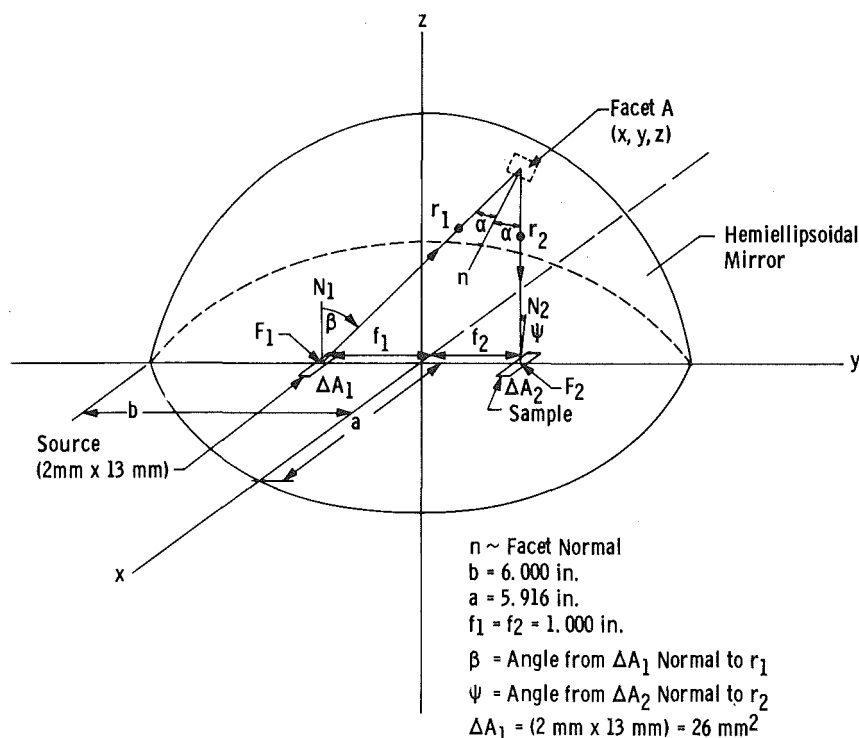
Figure 12. Hemispherical coordinate system employed in Ray-Trace program.

once an arbitrary mirror facet location A(x, y, z) has been selected; then the image ΔA_2 of a given ΔA_1 can be mapped by rigorous ray tracing. By ray tracing, one can determine the magnification for the finite size areas as well as the degree of aberration of the image caused by the mirror. The ray-tracing equations for a hemiellipsoidal mirror are given in Ref. 7. Thus, the rectangular area ΔA_1 can be broken up into "point sources" that lie up to 0.65 cm from the mathematical location of F_1. For this study the area ΔA_1 was represented by 121 points about F_1, and each point ray traced, via an arbitrarily selected facet A(x, y, z) of the hemiellipsoidal mirror, into the z = 0 plane about F_2. This was repeated for 25 different locations of the facet A(x, y, z). The ray tracing was performed with the aid of an IBM 370/155 computer, and the results were displayed on an IBM cathode ray tube plotter. The resulting plots for two facets located at coordinates (3.50 in., -3.50 in., 3.29 in.) and (3.50 in., 3.50 in., 3.29 in.), respectively, are shown in Figs. 13 and 14, where the magnification and demagnification character-istics of the mirror are graphically illustrated. The only difference in the two cases is that in Fig. 13, y = -3.50, whereas in Fig. 14, y = +3.50. In both cases the rectangular image at the conjugate foci (F_2) is some-what skewed. The CRT plots provided a means for determining the area

Hemiellipsoid Ray Trace

x = 3.50 in. r_1 = 5.417 in.   β = 52.4 deg
y = -3.50 in. r_2 = 6.583 in.   ψ = 60 deg
z = 3.29 in.   γ = 125.5 deg
                                           ζ = 142.4 deg
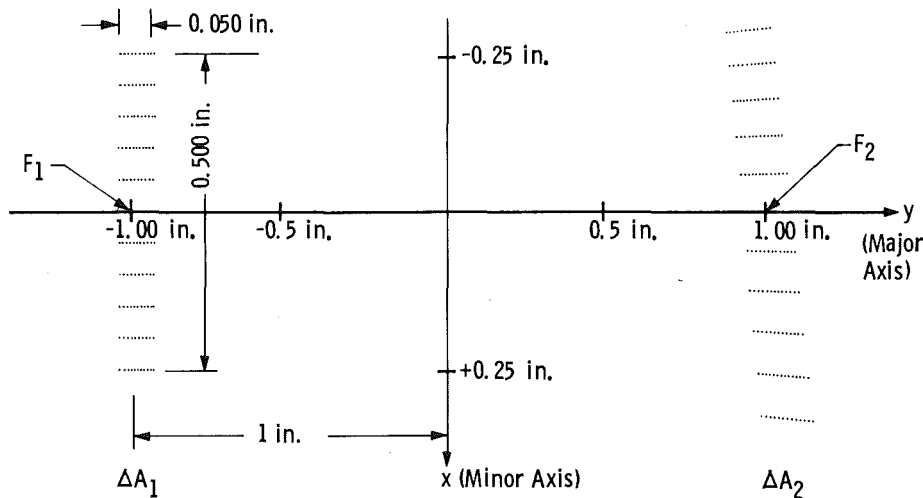
Figure 13. Ray trace for facet located at 3.50, -3.50, and 3.29.

ΔA_2 (area ΔA_1 is preselected) since the outline of the image formed about F_2 can be planimetered to an accuracy of 0.5 percent. Since Eq. (32) must be satisfied in order to insure diffuse irradiation of the sample for finite areas, it is necessary to substitute the computed values of β, ψ, and ΔA_1, along with the measured (planimetered) value of ΔA_2 back into Eq. (32). It was found that the right and left sides of Eq. (32) agreed to within 2 percent. Thus, it has been confirmed that the hemiellipsoidal mirror can be employed as an optical system to collect radiation from a finite size diffuse source centered about F_1 and focus the radiation so that a sample centered at F_2 is diffusely illuminated. Also, with ΔA_1 known (chosen as the area of monochromator slit) and ΔA_2 measured, the area magnification for the finite areas case can be defined [in a manner similar to that of Eq. (19)] as

$$M(\beta,\gamma) = \frac{\Delta A_2}{\Delta A_1}$$

(33)

From Eq. (33) the area magnification for finite areas (actual case) can be compared with the results of the ideal case of infinitesimal areas [Eq. (19)].

Hemiellipsoid Ray Trace

x = 3.50 in.	r_1 = 6.583 in.	β = 60 deg
y = 3.50 in.	r_2 = 5.417 in.	ψ = 52.41 deg
z = 3.29 in.		γ = 37.87 deg
		ζ = 54.92
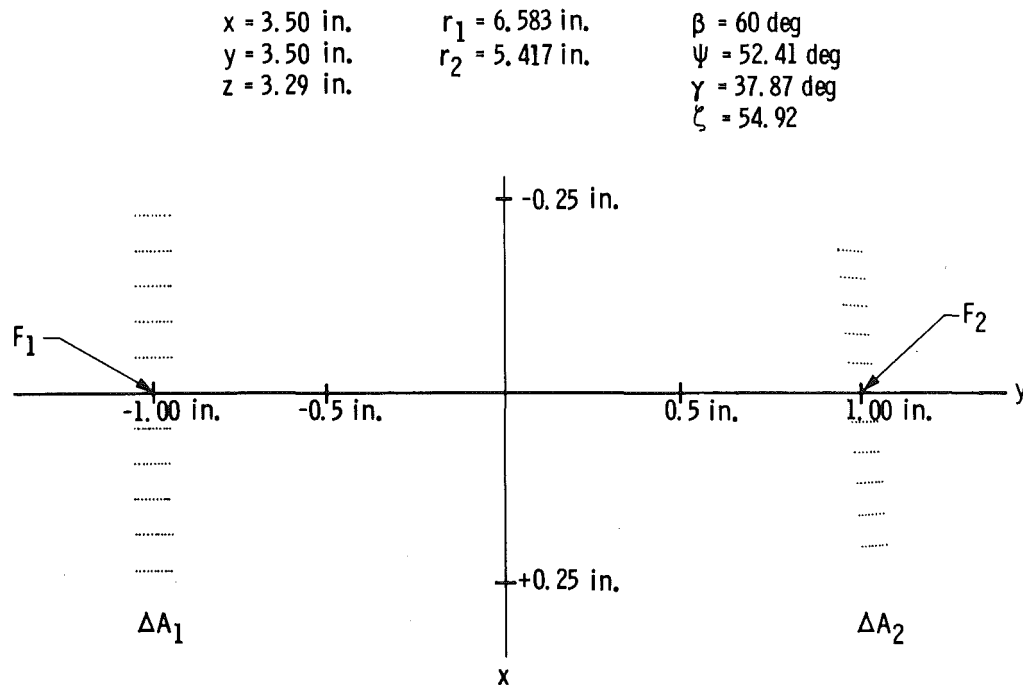
Figure 14. Ray trace for facet located at 3.50, 3.50, and 3.29.

4.2.3 Experimental Determination of the Hemi-Ellipsoidal Mirror Focusing Characteristics

In order to study experimentally the focusing properties of the mirror, the arrangement shown in Fig. 15 was utilized. A pinhole light source 3/32-in. in diameter was placed at one foci, and photographic film was stretched across the other foci for photographing the light source image. The pinhole is the smallest practical area that could be used and still give assurance of approaching being "infinitesimal." The light source was covered with various baffles inclined at angles β of 0, 15, 30, 45 and 60 deg as measured from the normal to the light source. The baffles were 2 in. long with an ID of 3/8 in., which resulted in an irradiation solid angle of 0.0154 sr and an angular spread of 4 deg. The entire light source and baffle were rotated about the source normal at F_1 to obtain data at azimuthal angles, γ, of 0, 90, 180, and 270 deg (see Fig. 15). This allowed both in-plane measurements (the plane containing the source normal and both foci) and out-of-plane measurements. Out-of-plane measurements corresponded to γ values of 90 and 270 deg. For γ = 180 deg
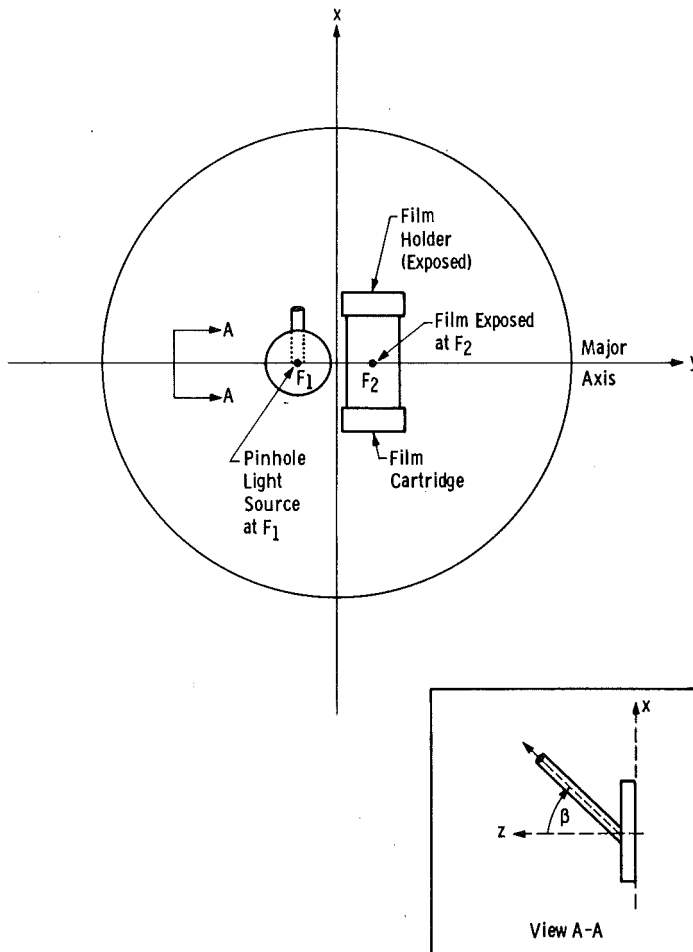
Figure 15. Apparatus for experimental determination of ellipsoid focusing properties (rear view).

the baffle was in-plane but pointing away from the conjugate foci (see Fig. 15), whereas for $\gamma = 0$ the baffle was pointing in the general direction of the conjugate foci. Photographs were made for each combination of β and γ mentioned previously; two typical photographs of the pinhole image at the conjugate foci are shown in Figs. 16a and b. After magnification by a factor of 18.7, the photographs were planimetered to obtain the areas for the different conditions. In this manner the area magnification, $M(\beta, \gamma)$, of the hemiellipsoidal mirror as a function of direction was determined by knowing exactly the area of the 3/32-in.-diam source pinhole. The area magnification results are presented in Table 1. Values of $M(\beta, \gamma)$ greater than 1 represent magnification, and values less than 1 represent demagnification. Demagnification was observed for $\gamma = 0$ and $\beta = 15$, 30, 45, and 60 deg, whereas magnification

was obtained for the other γ directions (γ = 90, 180, and 270 deg) observed. For the out-of-plane measurements, γ = 90 and 270 deg, and the magnification is essentially constant as a function of β with an average magnification value of about 1.22 obtained.

a. β = 60 deg, γ = 0
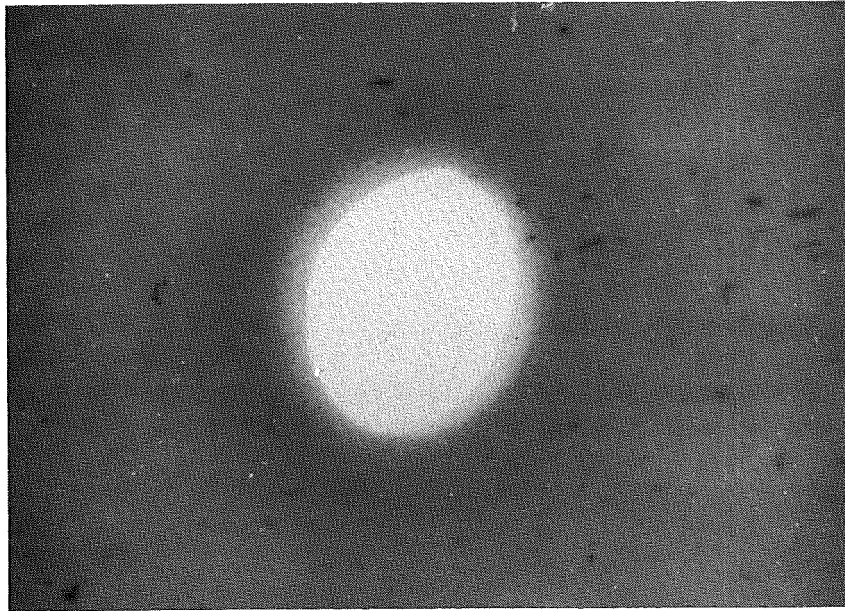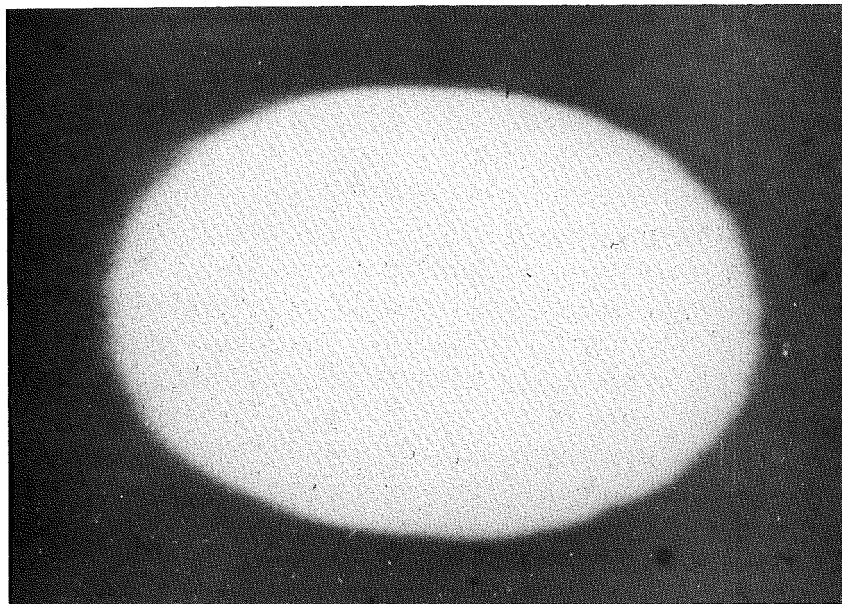
b. β = 60 deg, γ = 180 deg
Figure 16. Pinhole light image at conjugate foci.

Table 1. Experimental Magnification Data,
$M(\beta,\gamma)$

β	γ, deg			
	0	90	180	270
0	1.26	1.26	1.26	1.26
15	0.90	1.24	1.56	1.25
30	0.72	1.26	1.75	1.21
45	0.58	1.11	2.20	1.32
60	0.50	1.26	2.69	1.08

In order for the hemiellipsoidal mirror to produce diffuse irradi-
ation of the sample area it is necessary that the experimental values
of $M(\beta,\gamma)$ agree with the analytically derived requirements. The
value $M(\beta,\gamma)$ as determined from Eqs. (19) and (33) and the experi-
mental data are each shown in Fig. 17 as a function of β for $\gamma = 0$ and
180 deg. For an area magnification of unity [$M(\beta,\gamma) = 1$], the analyti-
cal results show that the radiation must be emitted from F_1 at approxi-
mately $\beta = 9.5$ deg ($\gamma = 0$). For $\beta = 9.5$ deg ($\gamma = 0$), ΔA_1 is demagnified
[$M(\beta,\gamma) < 1$], and for $\beta < 9.5$ deg ($\gamma = 0$ or 180 deg), ΔA_1 is magnified
[$M(\beta,\gamma) > 1$]. The analytical results show the relationship between
$M(\beta,\gamma)$ and β which must exist in order to ensure diffuse irradiation at
F_2 and the validity of Eq. (18). The infinitesimal areas requirements
and the finite areas (ray-trace) analysis are seen to be in excellent
agreement. This means that finite areas the size of the monochromator
entrance slit approach behaving as ideal infinitesimal areas. Likewise,
the experimental data shown in Fig. 17 also agree very well with the
theory; the two are within 8 percent of one another. This agreement of
the experimental data with the theoretical requirements proves that for
a diffuse source located at F_1 (Fig. 12), the hemi-ellipsoidal mirror
will indeed diffusely irradiate a sample located at F_2.

Figure 18 shows a comparison of the infinitesimal areas theory,
Eq. (19), and the experimental data at various γ locations where γ is
measured as shown in Fig. 11. Good agreement between theory and
data is shown in Fig. 18 for out-of-plane data ($\gamma = 90$ or 270 deg). The
theory and data both show that for directions to the right of a plane
passing through the source normal and perpendicular to the plane con-
taining the major axis and the sample normal ($0 \leq \gamma < 90$ deg and

270 deg $< \gamma \leq 360$ deg), $M(\beta, \gamma)$ increases as the angle away from the source normal, N, increases and for directions to the left of this plane (90 deg $< \gamma < 270$ deg) that $M(\beta, \gamma)$ decreases for increasing angles away from the source normal. The agreement of the data with the theoretical requirements for three-dimensional hemispherical irradiation proves that the hemiellipsoidal mirror does cause the sample to be diffusely irradiated.

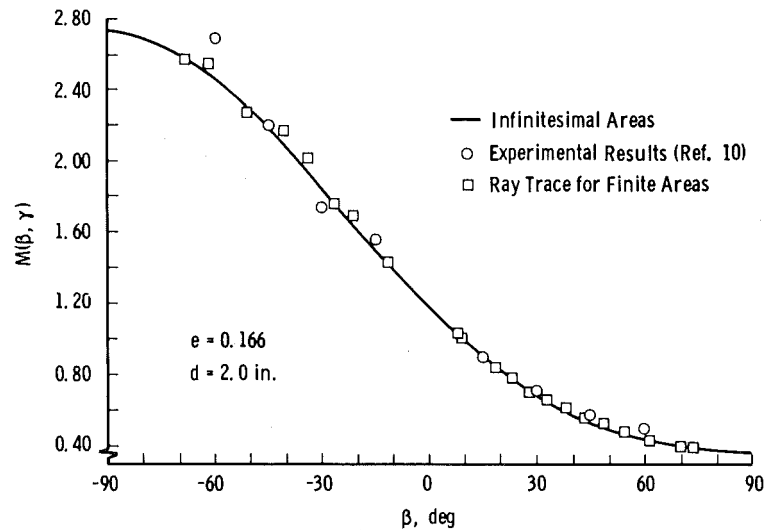Figure 17. Comparison of magnification results for infinitesimal areas, experimental data, and finite areas as a function of β for $\gamma = 0$ and 180 deg.
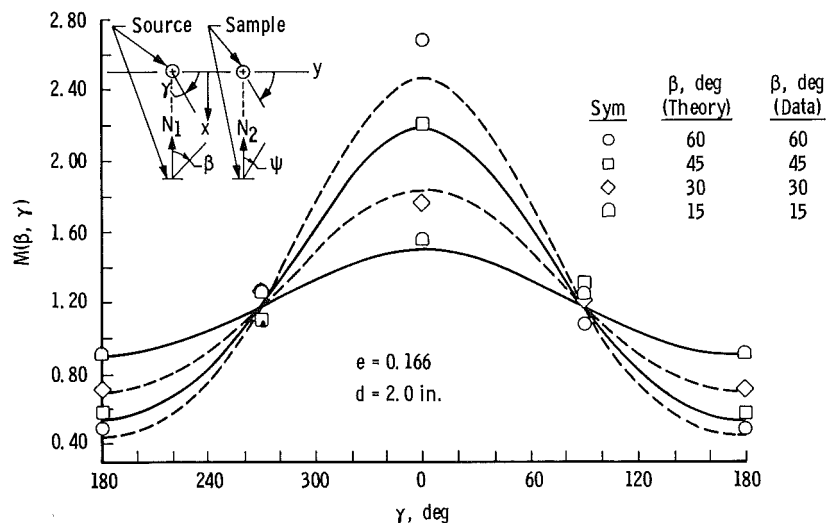
Figure 18. Magnification as a function of azimuthal angle γ and polar angle β.
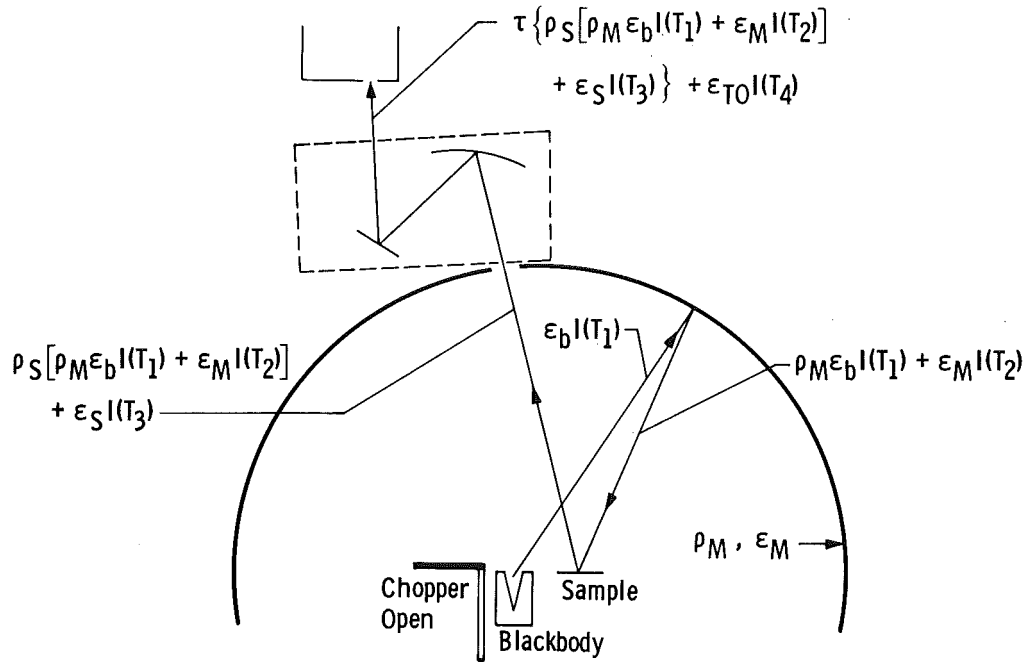
31

4.3 SUMMARY OF PERFORMANCE REQUIREMENTS

The purpose of Section 4.0 has been to state the requirements necessary for the hemi-ellipsoidal infrared reflectometer to be used for measuring ρ_{hd}. The two requirements were then shown to be experimentally fulfilled. First the blackbody source was shown to approach being an ideal blackbody both from a cosine power distribution (Fig. 8) and a constant intensity distribution (Fig. 7). Once an acceptable blackbody source had been established, the theoretical focusing properties of a perfect hemi-ellipsoidal mirror were defined based on ideal infinitesimal source and sample areas. A finite areas analysis of the mirror was then performed via a rigorous ray-trace method (Ref. 7). The finite areas source and sample results were shown to be in excellent agreement with the ideal infinitesimal areas requirements (Fig. 17). Finally, experimental data obtained in the hemi-ellipsoidal reflectometer were compared with the analytical requirements, and both were shown to be in good agreement. This yields the conclusion that for a diffuse source located at one foci of the mirror, the mirror will focus diffuse radiation at the sample foci. Thus, both requirements for measuring ρ_{hd} have been experimentally fulfilled. Reflectance data employing this system will be presented in Section 8.0.

5.0 CHOPPER BLADE HEATING PROBLEMS
(FOR VACUUM OPERATION)

Since the chopper blade is positioned in close proximity to the mouth of the blackbody (≈ 0.2 in.), the chopper blade will undoubtedly heat up if operated in a vacuum. Convection cooling will be absent since the components will be in a vacuum of 10^{-6} torr or less. The question that arises is what effect if any the heating of the chopper blade will have on the detector output and in particular on the determination of the sample reflectance. Also, what role, if any, will the radiation from other components play? The different surfaces affecting the radiation incident on the detector are shown schematically in Figs. 19a and b. In Fig. 19a the chopper blade is in the open position, letting the radiation emitted by the blackbody through, and in Fig. 19b the chopper blade is in the closed position with the blackbody blocked off, but now the chopper blade is emitting. The sources of radiation that the detector receives are from the blackbody emitting at T_1, the ellipsoidal mirror emitting at T_2, the sample emitting at T_3, the transfer optics emitting at an effective temperature of T_4, the chopper

emitting at T_5, and the reference surface emitting at T_6. The transfer optics shown in Fig. 19 are two mirrors, but the transfer optics could also be considered to include the chamber window and the monochromator mirrors and prism in front of the detector.

$$\tau\left\{\rho_S\left[\rho_M\varepsilon_b I(T_1) + \varepsilon_M I(T_2)\right] + \varepsilon_S I(T_3)\right\} + \varepsilon_{TO} I(T_4)$$

$$\rho_S\left[\rho_M\varepsilon_b I(T_1) + \varepsilon_M I(T_2)\right] + \varepsilon_S I(T_3)$$

$\varepsilon_b I(T_1)$

$\rho_M\varepsilon_b I(T_1) + \varepsilon_M I(T_2)$

ρ_M, ε_M

Chopper Open   Sample   Blackbody

a. Chopper open

$$\tau\left\{\rho_S\left[\rho_M\varepsilon_c I(T_5) + \varepsilon_M I(T_2)\right] + \varepsilon_S I(T_3)\right\} + \varepsilon_{TO} I(T_4)$$

$\varepsilon_c I(T_5)$

$\rho_M\varepsilon_c I(T_5) + \varepsilon_M I(T_2)$

$$\rho_S\left[\rho_M\varepsilon_c I(T_5) + \varepsilon_M I(T_2)\right] + \varepsilon_S I(T_3)$$

Chopper Closed   Sample   Blackbody
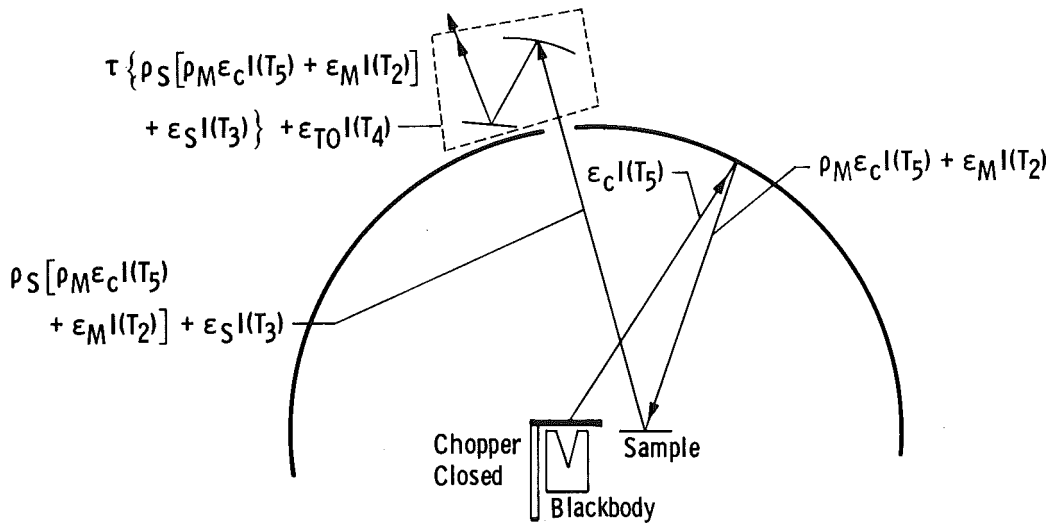
b. Chopper closed

Figure 19. Radiation components seen by detector.

33

Consider now Fig. 20. The ordinate scale represents the detector output in volts. This output is directly proportional to the radiative power reaching the detector from all sources within the optical path. When the reference surface is a near-perfect reflector, the detector output with the chopper blade in the open position will be given by

$$B_{R1} = K[\epsilon_b I_b(T_1)\rho_M\rho_{Ref}\tau + \rho_{Ref}I_M(T_2)\epsilon_M\tau + \epsilon_{Ref}I_{Ref}(T_6)\tau + \epsilon_{TO}I_{TO}(T_4)] \cos \theta \, d\omega_R \quad (34)$$

In Eq. (34) K is the detector calibration constant (responsivity) in v/w. All the terms in Eq. (34) and throughout this discussion are spectral quantities, but the λ notation was omitted to keep the equations from being too cumbersome. The first term inside the brackets is the power emitted by the blackbody at temperature T_1, which is reflected from the ellipsoidal mirror, reflected from the reference surface, and transmitted through the transfer optics at an efficiency τ. Similarly, the second term represents the power emitted by the ellipsoidal mirror at T_2 that is reflected from the reference surface and eventually reaches the detector. The third term is the power emitted by the reference surface at T_6 that reaches the detector after passing through the transfer optics. The final term is the power emitted by the transfer optics at T_4 that reaches the detector. The sum of the last three terms in Eq. (34) is equivalent to u_1 in Fig. 20.
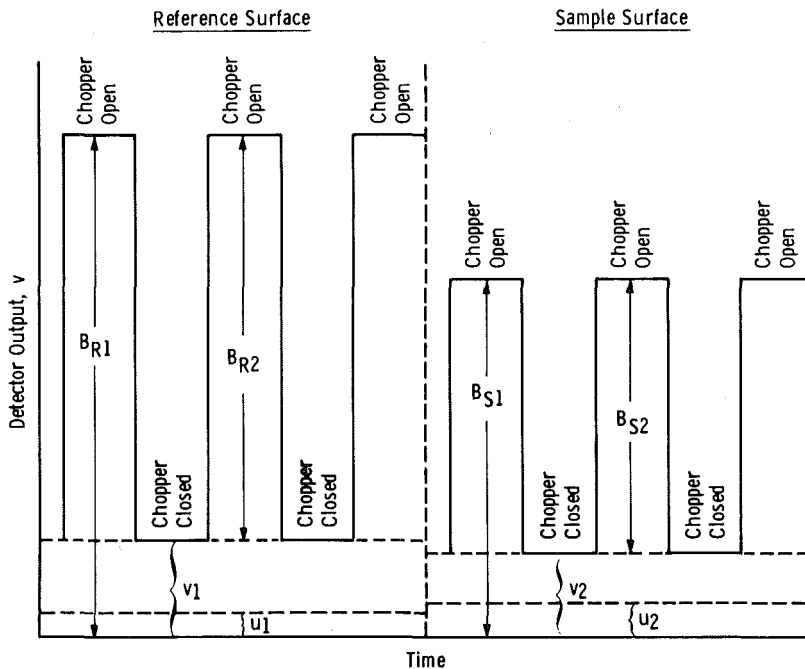

Figure 20. Detector output versus time for reference and sample surfaces.

When the chopper blade is in the closed position, the detector output for the reference surface is given by v_1 where

$$v_1 = K[\epsilon_c I_c(T_5)\rho_M \rho_{Ref}\tau + \rho_{Ref}I_M(T_2)\epsilon_M \tau + \epsilon_{Ref}I_{Ref}(T_6)\tau + \epsilon_{TO}I_{TO}(T_4)] \cos\theta \, d\omega_R \quad (35)$$

The last three terms in Eq. (35) are identical to those in Eq. (34). The first term is the power emitted by the chopper blade at T_5 that is reflected from the ellipsoidal mirror and reference surface that reaches the detector. In Fig. 20 the chopper blade-emitted power is equivalent to $v_1 - u_1$.

Expressions similar to Eqs. (34) and (35) can be formulated for the sample surface. For the chopper blade open, the detector output is given by

$$B_{S1} = K[\epsilon_b I_b(T_1)\rho_M \rho_S \tau + \rho_S \epsilon_M I_M(T_2)\tau + \epsilon_S I_S(T_3)\tau + \epsilon_{TO}I_{TO}(T_4)] \cos\theta \, d\omega_R \quad (36)$$

For the chopper blade closed, the detector output is given by

$$v_2 = K[\epsilon_c I_c(T_5)\rho_M \rho_S \tau + \rho_S \epsilon_M I_M(T_2)\tau + \epsilon_S I_S(T_3)\tau + \epsilon_{TO}I_{TO}(T_4)] \cos\theta \, d\omega_R \quad (37)$$

where ρ_S and ϵ_S are the reflectivity and emissivity of the sample surface. Notice in Fig. 20 the peak to valley amplitude for the reference surface is B_{R2} rather than B_{R1}, so a phase-sensitive lock-in amplifier would respond to B_{R2} rather than B_{R1} since the v_1 portion of the reference output would essentially be a d-c output, which the amplifier would not respond to. It is the B_{R2} value that is used in the reflectance measurements. Similarly, for the sample surfaces, the output which the amplifier responds to is B_{S2} rather than the B_{S1}, and v_2 is a d-c component which is filtered out by the lock-in amplifier. So the question arises whether $B_{S2}/B_{R2} = \rho_S/\rho_{Ref}$. From Fig. 20, the a-c component for the reference surface is given by $B_{R2} = B_{R1} - v_1$, and from Eqs. (34) and (35) this reduces to

$$B_{R2} = \rho_M \rho_{Ref}\tau[\epsilon_b I_b(T_1) - \epsilon_c I_c(T_5)] \cos\theta \, d\omega_R \quad (38)$$

Similarly for the sample surface,

$$B_{S2} = B_{S1} - v_2 = \rho_M \rho_S \tau[\epsilon_b I_b(T_1) - \epsilon_c I_c(T_5)] \cos\theta \, d\omega_R \quad (39)$$

The ratio of the two a-c components then yields

$$\frac{B_{S2}}{B_{R2}} = \frac{\rho_M \rho_S [\epsilon_b I_b(T_1) - \epsilon_c I_c(T_5)] \tau \cos\theta - d\omega_R}{\rho_M \rho_{Ref} [\epsilon_b I_b(T_1) - \epsilon I(T_5)] \tau \cos\theta \ d\omega_R} \tag{40}$$

or

$$\frac{B_{S2}}{B_{R2}} = \frac{\rho_S}{\rho_{Ref}} \tag{41}$$

This result shows that the chopper blade temperature increase will not affect the determination of the ratio of the two signals directly. From Eq. (40), however, it is apparent that the a-c signal amplitude would be decreased by the chopper blade heating.

6.0 SAMPLE REFLECTANCE EFFECTS

In an ellipsoidal mirror, radiation reflected from a surface located at one foci will in turn be refocused at the other foci. The result generally is that the radiation makes multiple passes between surfaces located at the two foci until all of the radiation is absorbed. It is apparent that these multiple reflections could cause an error in the reflectance determination since multiple reflections effectively cause a higher incident intensity. This problem is eliminated if either of the two surfaces is a blackbody (has zero reflectance). In this study the source of radiation was a blackbody, and this eliminated the multiple reflection problem. However, the power reflected back to the blackbody from the first reflection off the sample does depend on the sample reflectance, and the blackbody equilibrium temperature is a function of the amount of re-reflected radiation. Nearly all of the radiation emitted by the blackbody and focused on the sample will be returned to the blackbody when a gold reference mirror is in the sample position, whereas only 4 to 5 percent will be returned from a black surface. It was found that a blackbody equilibrium temperature of 867°F was observed when the gold reference mirror was used, whereas a temperature of 852°F was obtained for a black surface. This 15°F temperature difference means the blackbody intensity incident on the gold surface is somewhat higher than that for the black surface. To make relative reflectance measurements the incident intensity has to be the same. The error would result in reflectance values that were too low with the greatest error being for the shorter wavelengths. The easiest method of eliminating this problem was to

reduce the sample irradiated area. This was done by masking the sample irradiated area to a slot 3/16 in. x 3/4 in., which was slightly larger than the monochromator entrance slit. This reduced the irradiated area (see Fig. 5) by a factor of about 5. This caused, in the worst condition, only about 1.5°F change in the blackbody operating temperature, and this change was essentially undetectable (less than 0.5-percent change), when the radiation output was observed. The mask essentially eliminated this problem, and all the data reported in this report were obtained with the mask in place.

Another question of concern was the possibility of different electonic waveforms being generated for the reference surface (specular surface) and for a diffuse surface such as MgO. For the specular surface, only a small irradiated portion of the ellipsoidal mirror is actually used; thus, the chopper blade has only to move through a small angle to completely open or completely close the detector from the blackbody as seen through the specular reference. In contrast, a diffuse surface reflects a portion of the radiation from all directions into every direction. In this case the chopper blade has to completely block the entire blackbody off so that no radiation is emitted into the hemisphere for the closed position, and similarly the chopper blade must completely clear the blackbody for the open case. In order to determine if there was a problem, the output of the preamplifier was tapped into an oscilloscope, and the output waveform for a specular sample was compared to that for a diffuse surface. Typical results are shown in Fig. 21. The waveform is not a square wave because of (1) the relatively slow thermocouple response and (2) the capacitive coupling to the preamplifier. The right-hand a-c

Relative Volts

MgO Sample (Diffuse)
$\lambda = 1.5\,\mu m$

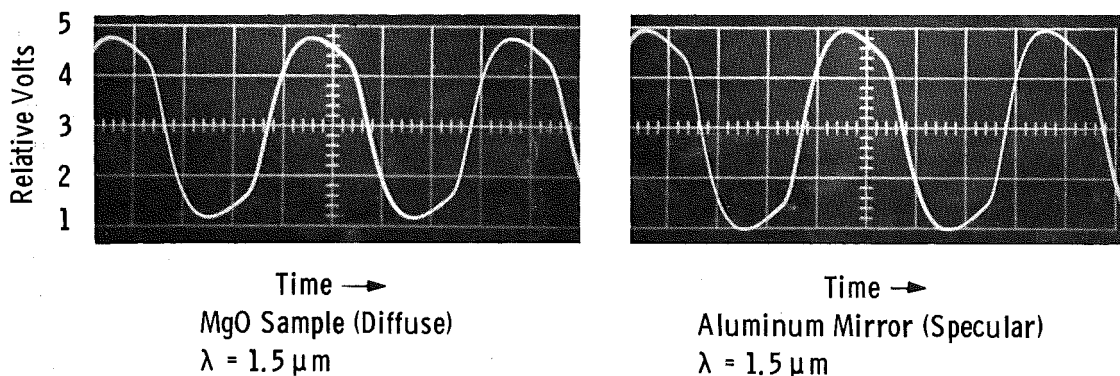Aluminum Mirror (Specular)
$\lambda = 1.5\,\mu m$

Figure 21. Waveforms observed for a diffuse MgO sample and a specular aluminum mirror.

waveform in Fig. 21 was for a freshly coated aluminum mirror surface with the preamp gain adjusted to obtain a peak height of 1.0 on the oscilloscope scale. The left-hand a-c waveform shows the output for an MgO surface, which is a well known diffuser. The wavelength used for these results was 1.5 μm. As can be observed, the waveform shapes are identical, and the peak height of the MgO is approximately 90 percent of that for the polished aluminum, indicating the approximate reflectance of MgO. From these observations, it is concluded that no problem exists regarding different waveforms for the two types of surfaces.

7.0 PROCEDURE

Before a reflectance measurement was made, the hemi-ellipsoidal mirror alignment was established. The hemi-ellipsoid, test surface, blackbody, transfer optics and spectrometer were aligned using a diffuse sample surface. It was found that the focusing for a diffuse surface was much more critical than for the specular case. For the diffuse surface, radiation from the entire hemi-ellipsoid must be in focus, whereas for the specular case only a small portion of the mirror is utilized. Alignment was established by passing the mercury green line (0.5460 μm) through the spectrometer and focusing it on the diffuse sample. The reflected radiation was re-imaged at the center of the blackbody. The blackbody, test surface, and hemi-ellipsoid were aligned first, and the spectrometer and transfer optics were adjusted to match.

After the blackbody had been allowed to come to equilibrium temperature, the reference surface (gold-coated mirror) was located at the test surface foci. The detector output was then recorded as a function of wavelength. After the test surface had been substituted for the reference mirror, another scan of detector output versus wavelength was made. Reflectance values were then obtained by ratioing the detector outputs at specific wavelengths as determined by the drum number and wavelength marker of the monochromator. In all cases the reflectance is presented relative to the reflectance of the gold mirror. However, the reflectance of gold is 99 percent or greater for wavelengths of 2 μm and longer (Ref. 8), so the absolute reflectance is not more than 1 percent less than the relative values presented.

8.0 RESULTS

To demonstrate that the reflectometer was functioning satisfactorily, several surfaces were investigated. Measurements reported from 2 to 25 μ were obtained using a KBr prism and measurements from 15 to 34 μ were obtained using a CsBr prism. (Note: None of the results was corrected for the mirror hole loss.) Figures 22 and 23 show the reflectance of two diffuse coatings which have been used or proposed previously as infrared integrating sphere coatings—sulfur and cesium iodide. The sample holders were made of aluminum and had a cavity 1/8 in. deep for holding the sample material. As can be seen, sulfur is not a good choice for an infrared sphere coating due to its many absorption bands and an overall relatively low reflectance as compared to the cesium iodide. The reflectance of a material such as sulfur cannot be measured in a heated cavity reflectometer because of its low thermal conductivity and its low melting point. Cesium iodide,
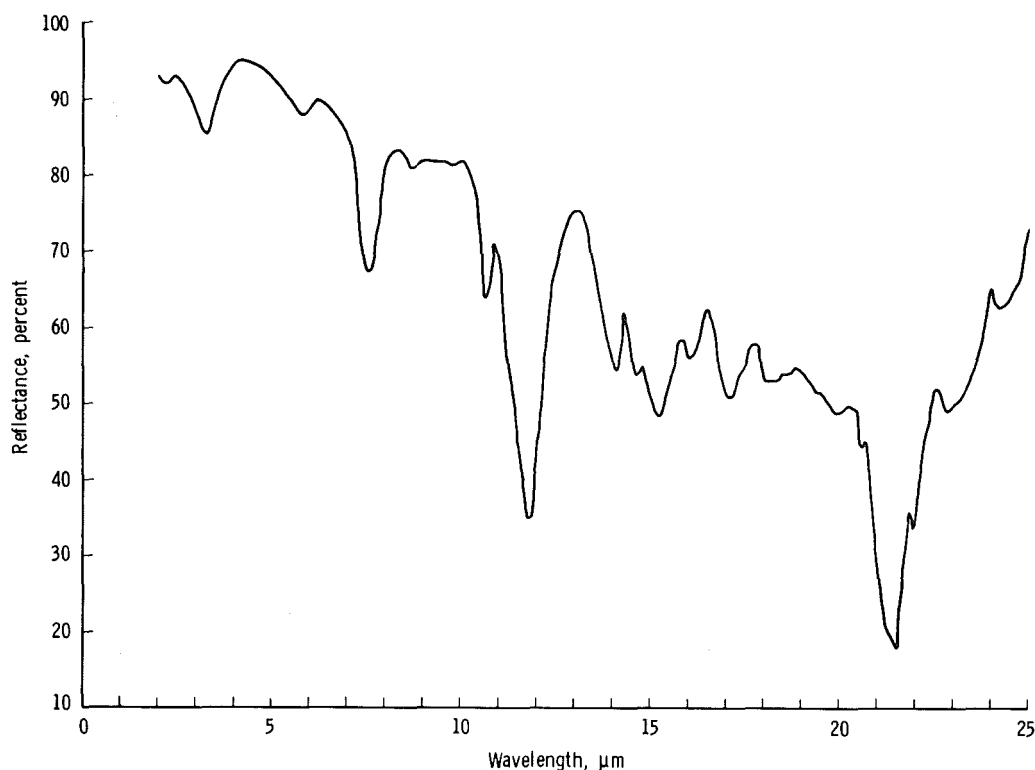
Figure 22. Reflectance of flowers of sulfur sample, θ = 15 deg.

on the other hand, has a reflectance of 80 percent or greater over essentially the full range from 2 to 25 μ. The cesium iodide was of 99.99-percent purity and was ground into a fine powder before being pressed into the sample holder. The reflectance measurements were made with the cesium iodide at near room temperature. A bakeout of the sample as suggested in Ref. 9 might have increased the reflectance by decreasing the water content, but this was not done.
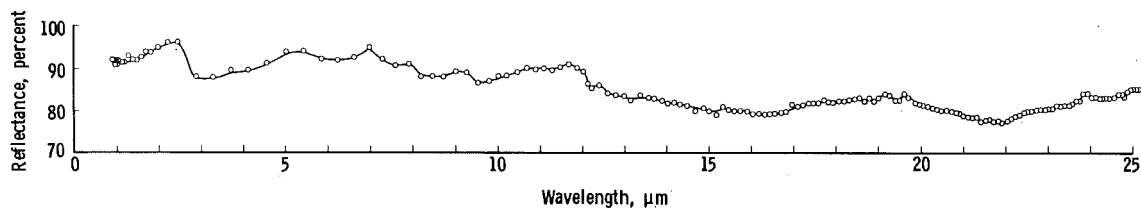

Figure 23. Reflectance of ground cesium iodide sample, θ = 15 deg.

Figures 24 and 25 show the results of reflectance measurements for a gold-coated grit sample. The sample was prepared by covering a fresh epoxy-coated surface with No. 180 silicon carbide grit. After the epoxy hardened, another very thin layer of epoxy was applied over
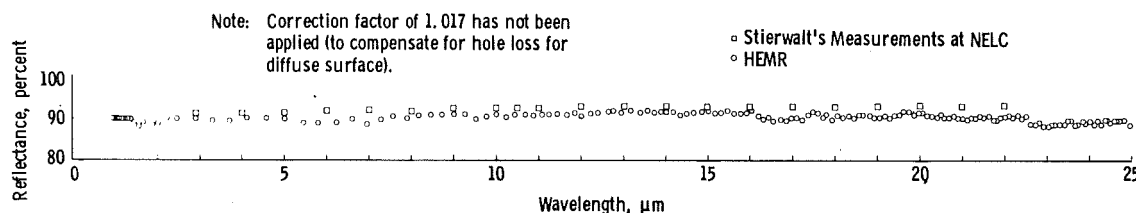

Figure 24. Reflectance of gold-coated grit sample (λ = 2 to 25 μ), θ = 15 deg.

the grit surface. This time after the epoxy hardened, the surface was overcoated with vacuum-deposited gold. This produced a rough surface (rms surface roughness σ = 7 to 10 μm, which was essentially diffuse for infrared radiation (Ref. 10). As can be seen in Fig. 24, the data were compared with measurements made by Dr. D. L. Stierwalt out to 22 μm at the Naval Electronics Laboratories Center, San Diego, California. Good agreement is seen for the two quite different techniques for measurement. The gold diffuser has a reflectance of 90 to 92 percent which is nearly constant over the wide spectral range from 2 to 34 μm. The data shown from 15 to 34 μm, Fig. 25, were obtained using the CsBr prism. In Figs. 26 through 30 are shown reflectance data for three types of black paints: Nextel[®] Suede, Nextel Velvet, and Cat-a-lac[®] black. The Nextel Suede shows very little variation across the spectrum, whereas for the other two, reflectance peaks

40

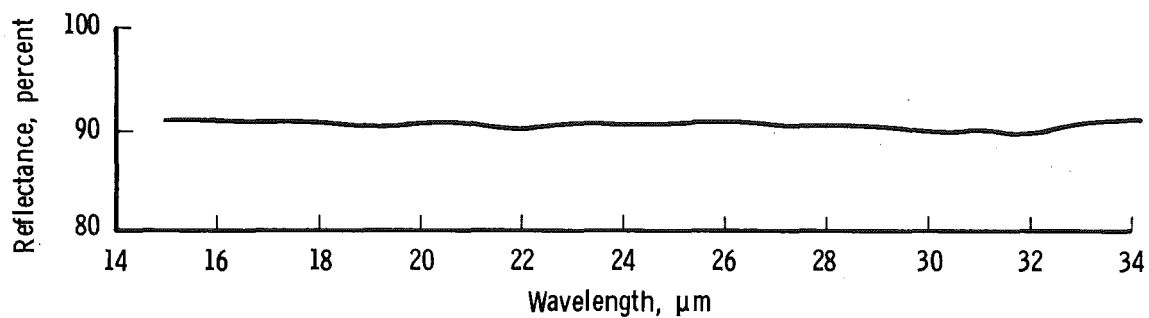**Figure 25.** **Reflectance of gold-coated grit sample (λ = 15 to 34 μ), θ = 15 deg.**
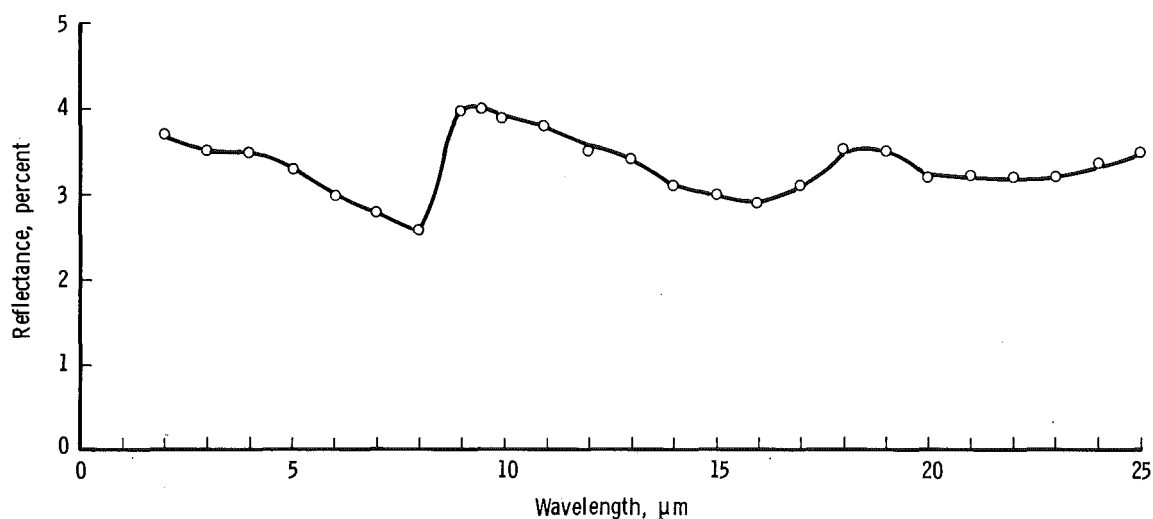
Figure 26. **Reflectance of black Nextel® Suede paint, θ = 15 deg.**
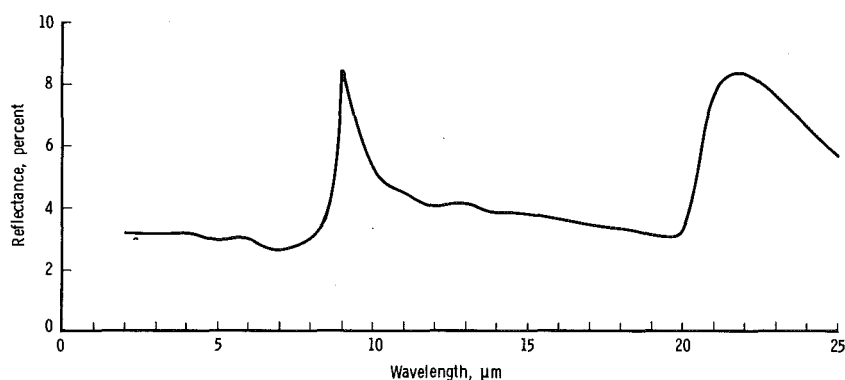

Figure 27. **Reflectance of black Nextel Velvet paint (2 to 25 μ), θ = 15 deg.**
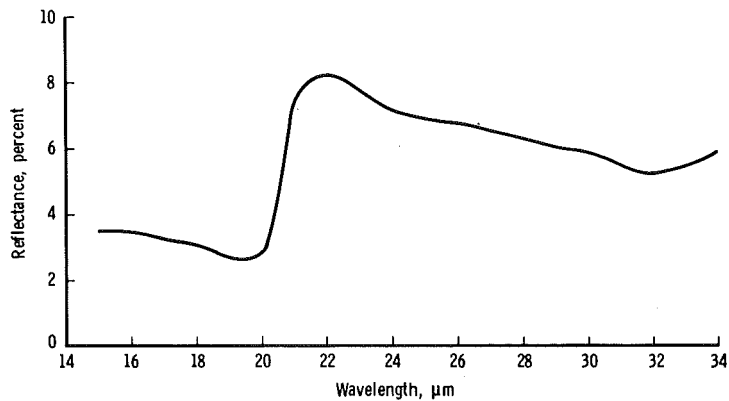
41

Figure 28. Reflectance of black Nextel Velvet paint (15 to 34 μ),
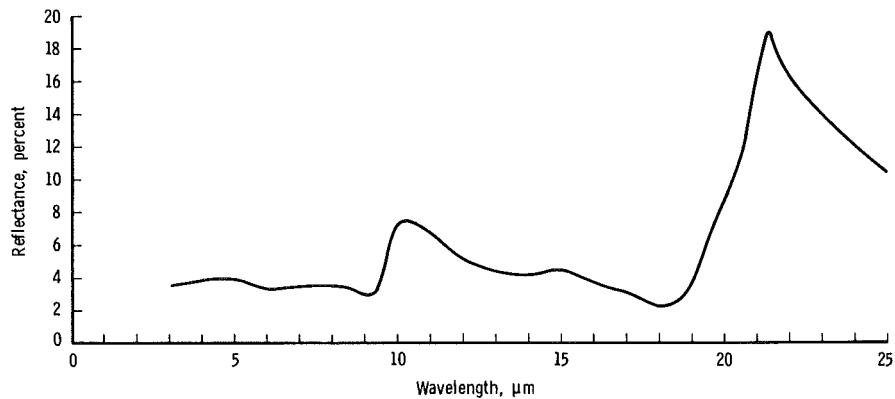θ = 15 deg.

Figure 29. Reflectance of Cat-a-Lac® black epoxy paint (2 to 25 μ),
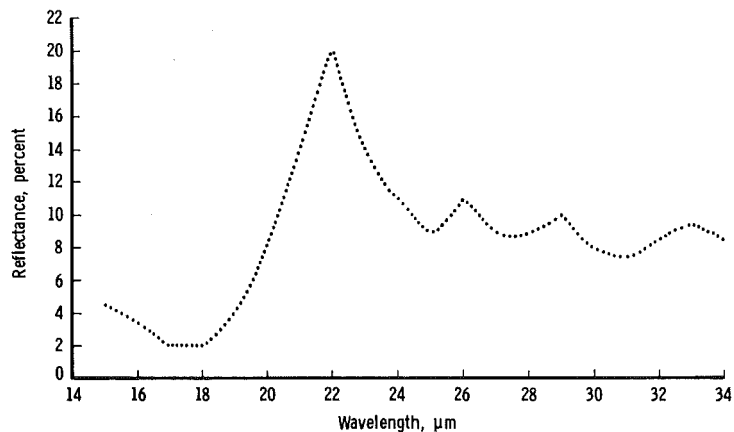θ = 15 deg.

Figure 30. Reflectance of Cat-a-Lac black epoxy paint (15 to 34 μ),
θ = 15 deg.

are observed in the vicinity of 9 and 22 μm; these peaks agree with the data of Stierwalt (Ref. 11) and Edwards (Ref. 12). Figure 31 shows the reflectance of a black carbon cloth which was used as a test surface in a recent test performed at AEDC. Although very black to the eye, the carbon cloth reflectance increases gradually with increasing wavelength from a value of about 5.5 percent at 2 μm to a peak value of 18.5 percent at 23 μm.
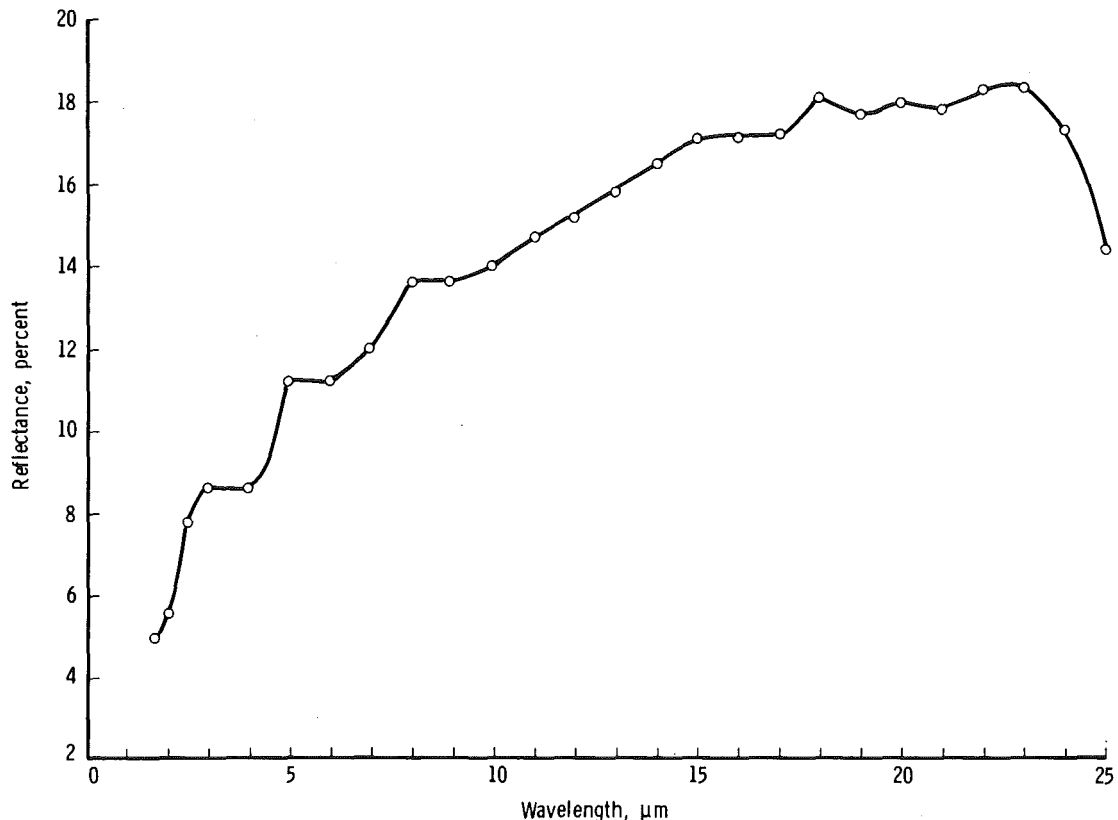
Figure 31. Reflectance of carbon cloth, θ = 15 deg.

Reflectance data for RTV-60® (red in color) and RTV-102® (white in color) are shown in Figs. 32 and 33, respectively. These data were taken to support aerodynamic heating tests in which model surface temperatures will be determined with the use of an infrared camera. The directional emissivities of the model surfaces have to be known in order for the temperatures to be determined. Since the reflectance capability of the HEMR is from 2 to 25 μm, it will be especially useful for infrared cameras operating in the 8- to 14-μm range as well as for those operating in the 2- to 5-μm range.
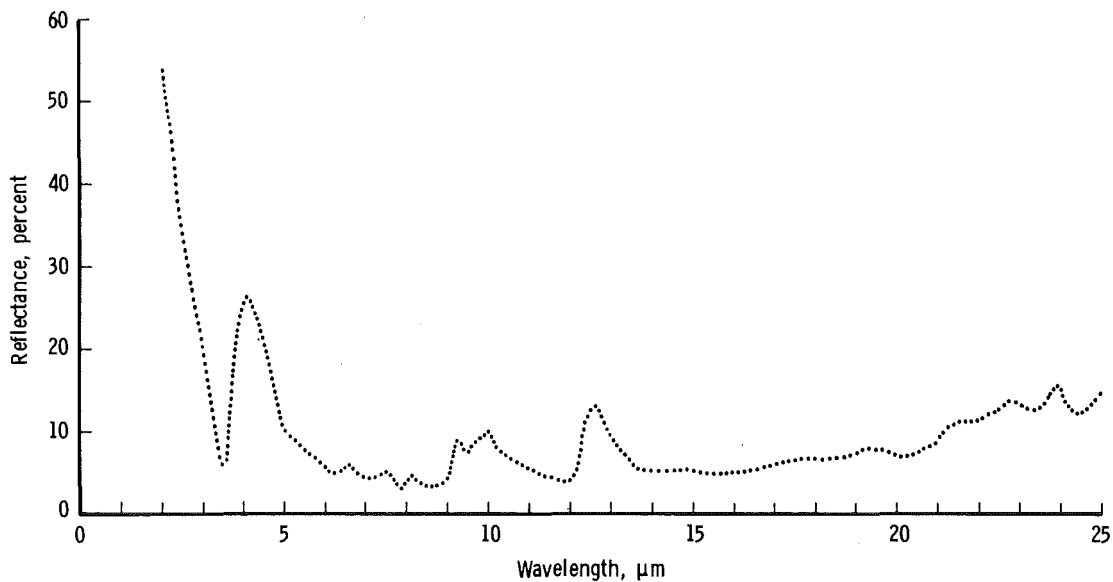
Figure 32. Reflectance of RTV-60® (red in color), θ = 15 deg.
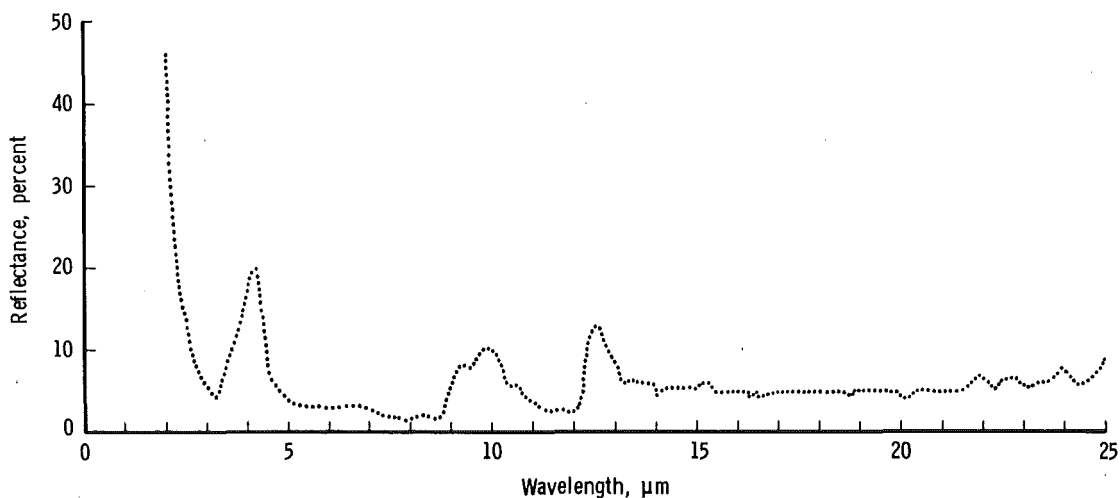
Figure 33. Reflectance of RTV-102® (white in color), θ = 15 deg.

A portion of the AEDC 12V chamber material was also measured for chamber thermal balance calculations. The chamber material is stainless steel with a chamber finish undefined, as it was pitted and uneven in places. The reflectance of this material is shown in Fig. 34 mainly to emphasize the varied usefulness and applications of the hemi-ellipsoidal mirror reflectometer in various aspects of testing at AEDC.
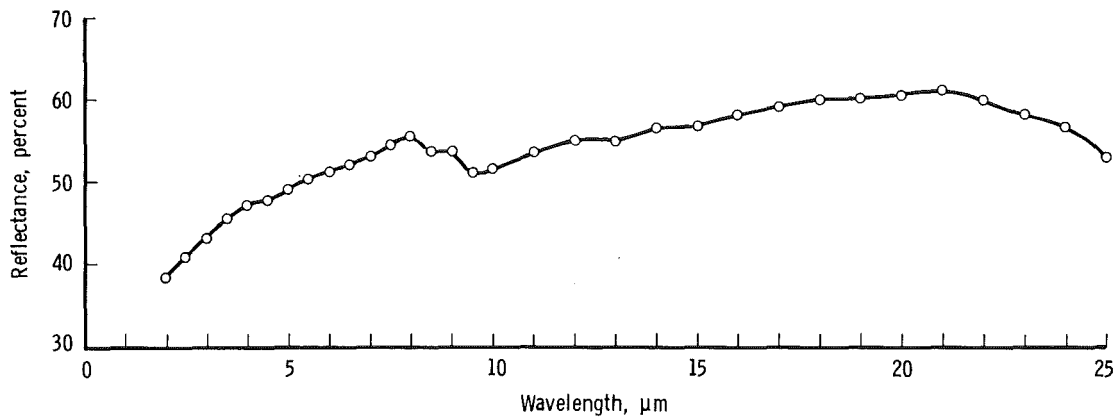
Figure 34. Reflectance of 12V chamber material (stainless steel), θ = 15 deg.

9.0 ERRORS

The possible sources of error associated with reflectance measurements in the HEMR are listed and discussed below.

1. Blackbody not a Perfect Diffuse Emitter. From Figs. 7 and 8 one can see that the distribution of the emitted blackbody radiation is nearly that of a diffuse emitter. Only at angles β > 80 deg or β < -80 deg is there any significant departure. The error introduced, if any, would be for nonspecular surfaces which would scatter radiation into directions between 80 and 90 percent. Even for a perfect diffuse emitter only 3 percent of the total emitted radiative power is contained in the directions 80 < β < 90 deg and -90 < β < -80 deg. Any error caused by this effect is therefore considered negligible.

2. Blackbody Absorptivity Less Than 1.0. To ensure that there were no problems associated with multiple reflections between the sample and blackbody sources, another blackbody (of the same type) was located at the sample foci and the reflectance measured. In the wavelength range from 2 to 20 μm, a reflectance value of 0.2 percent was the largest value obtained which yields an absorptivity of 0.998. Therefore, any error contribution from the blackbody not having an emissivity of exactly unity would be less than 0.002 in the sample reflectance value.

45

3. <u>Blackbody Temperature Instability.</u> The blackbody temperature is assumed equal for both sample and reference measurements. Any fluctuation could cause a discrepancy in the reflectance values, with the largest error being at the shorter wavelength ($\lambda < 2.0\ \mu$m) since the emissive power is a much stronger function of wavelength on the short wavelength side of the blackbody maximum. The blackbody temperature was stable within $\pm 1/2°$F which, for wavelengths longer than 2 μm, was undetectable from the emitted radiation detected. As pointed out in Section 6, however, the sample reflectance varying from 0.0 to 99.0 percent can cause a temperature increase of about 1.5°F even though the masks are in place. This increase for $\lambda > 2.0\ \mu$m is again negligible but could cause a small error if measurements at shorter wavelengths were attempted.

4. <u>Energy Loss Caused by the Hole in the Mirror.</u> The energy loss caused by the hole in the mirror will not affect specular reflectance determinations, but it definitely will be a factor for diffusing surfaces. For a diffuse blackbody the energy loss can be calculated from

$$F_{i-j} = \frac{\cos \beta_i \cos \beta_j A_j}{\pi r^2} = \frac{(1)(1)(2.01)}{\pi (6)^2} = \frac{2.01}{36\pi} = 1.76 \times 10^{-2} \tag{42}$$

where F_{i-j} is the form factor for determining energy leaving surface i (the blackbody) and hitting surface j (the hole in the mirror). A_j is the area of the hole in the mirror, β_i and β_j are the angles between the normals and the line connecting the two surfaces, and r is the radius of the HEM. Therefore, 1.76 percent of the energy emitted from the blackbody will be lost without ever being incident on the test surface. For a diffuse surface, the reflectance value measured should be multiplied by 1.0176. For surfaces having a reflectance of less than 10 percent this would be undetectable, but for highly reflecting surfaces this correction should definitely be considered. In order to apply this correction factor, however, it must be known that the surface is diffuse. In the infrared, where surfaces tend to become more specular, this becomes a problem, as this requires a knowledge of the sample bidirectional reflectance

before the application of the correction factor can be determined. Therefore, no corrections were made in this report for the hole loss.

5. Error Using a Gold Mirror as a Reference Surface. Since the reflectance of gold varies from approximately 99 percent to 99.5 percent over the range from 2 to 40 μ (Ref. 8), the reflectance values reported will be from 1/2 to 1 percent higher than the absolute reflectance based on this source of error alone.

6. Scattered Light in Monochromator. In single-pass instruments such as the monochromator used in this study, scattered light is an inherent problem. To reduce the scattered light at the longer wavelengths, a scatter plate was used for $\lambda > 12$ μm. The scattered light problem at the longer wavelengths was also reduced somewhat by the fact that the blackbody operating temperature was around 900°F; this means that the peak of the blackbody curve was at 3.85 μm, and therefore, less short wavelength energy was available for scattering. In general, the short wavelength radiation poses a greater scatter problem than does long wavelength radiation, but in this study the reverse was true. For wavelengths less than 1 μm the scattered longer wavelength radiation completely dominated the detector output, so measurements could not be made. The reason for this was, again, the steepness of the blackbody curve on the short wavelength side of the blackbody maximum (e.g., the emissive power at 1 μm is at most a factor of 10^{-4} times the maximum value). It is difficult to assign an error value to the reflectance measurements based on this problem since the scattered light error will depend on the reflectance of the sample surface being investigated.

7. Error Due to Finite-Sized Sample Areas. There was some concern about the focusing properties of the HEM, since the focusing is very critical. The equations for the HEM are based on infinitesimal areas, and it is well established that the aberrations and magnification increase as the distance from the foci increases. From the analytical studies for the infinitesimal areas and the ray-tracing investigation for finite areas in Section 4.0 it has been established that no problems exist for the small, finite-sized areas (2 x 13 mm) employed in this investigation.

The various major sources of error have been discussed. There is no way a definite error in measurement can be established. In general it is the belief of the authors that the reflectance measurements of specular surfaces are accurate to within ±1.5 percent and that the measurements of diffuse surfaces are accurate to within ±2.0 percent.

10.0 CONCLUSIONS

The design and operation of an ellipsoidal mirror reflectometer have been discussed. Several possible problem areas were investigated, and where necessary, solutions to the problems were found. The focusing characteristics of the ellipsoid were investigated both analytically and experimentally. It was firmly established that if the radiation source located at one foci emits diffusely, the test surface located at the other foci will also be irradiated diffusely; hence the requirement for making hemispherical-directional reflectance measurements was satisfied. Several samples were investigated and reflectance measurements made for wavelengths between 2 and 34 μm. Reflectance measurements for both specular and diffuse surfaces were obtained, and where comparisons were possible, good agreement was obtained with data found in the literature or with comparable measurements made at other laboratories. The ellipsoidal mirror reflectometer has been shown to have several advantages over other types of reflectometers. These advantages include the following: (1) the ellipsoidal mirror reflectometer has a broad wavelength range which is limited only by the detector and optical components; (2) there is no self-emission error such as is present in heated cavity reflectometers; (3) there are no polarization effects since all rays strike the ellipsoid at near-normal incidence; and (4) the mirror is versatile, as it can be used for measurements in a vacuum and, if desired, for cryogenically cooled samples.

REFERENCES

1. Wood, B. E., Smith, A. M., Roux, J. A., and Seiber, B. A. "Spectral Absolute Reflectance of CO_2 Frosts from 0.5 to 12.0 μ." AIAA Journal, Vol. 9, No. 7, July 1971, pp. 1338-1344.

2. Wood, B. E., Smith, A. M., Roux, J. A., and Seiber, B. A. "Spectral Infrared Reflectance of H_2O Condensed on LN_2-Cooled Surfaces in Vacuum." AIAA Journal, Vol. 9, No. 9, September 1971, pp. 1836-1842.

3. Neu, J. T. "Design, Fabrication, and Performance of an Ellipsoidal Spectroreflectometer." NASA-CR-73193, March 1968.

4. Neher, R. T. and Edwards, D. K. "Far Infrared Reflectometer for Imperfectly Diffuse Specimens." Applied Optics, Vol. 4, No. 7, July 1965, pp. 775-780.

5. Brandenburg, W. M. "Focusing Properties of Hemispherical and Ellipsoidal Mirror Reflectometers." Journal of the Optical Society of America, Vol. 54, No. 10, October 1964, pp. 1235-1237.

6. Edwards, D. K. "Radiative Transfer Characteristics of Materials." Transactions of the ASME: Journal of Heat Transfer, Series C, Vol. 91, February 1969, pp. 1-15.

7. Heinisch, R. P., Bradac, F. J., and Perlick, D. B. "On The Fabrication and Evaluation of an Integrating Hemiellipsoid." Applied Optics, Vol. 9, No. 2, February 1970, pp. 483-487.

8. Bennett, Jean M. and Ashley, E. J. "Infrared Reflectance and Emittance of Silver and Gold Evaporated in Ultrahigh Vacuum." Applied Optics, Vol. 4, No. 2, February 1965, pp. 221-224.

9. Geist, Jon, Kneissl, Gerhart J., and Weidner, V. R. "High Purity Powdered CsI as a High Reflectance Infrared Diffuser." Applied Optics, Vol. 6, No. 7, July 1967, pp. 1280-1281.

10. Wood, B. E. and Smith, A. M. "An Investigation of Infrared Diffuser Surfaces." AEDC-TR-74-22 (AD779771), May 1974.

11. Stierwalt, D. L. "Infrared Spectral Emittance Measurements of Optical Materials." Applied Optics, Vol. 5, No. 12, December 1966, pp. 1911-1915.

12. Edwards, D. K. and Hall, William M. "Far Infrared Reflectance of Spacecraft Coatings." Thermophysics and Temperature Control of Spacecraft and Entry Vehicles. Volume 18 of Progress in Astronautics and Aeronautics, Edited by Gerhard B. Heller, Academic Press, New York, 1966, pp. 3-19.

NOMENCLATURE

A	Area, cm^2
a	Semiminor axis = 5.916 in.
B	Detector output, v
b	Semimajor axis = 6.0 in.
d	Distance between F_1 and F_2 = 2 in.
e	Eccentricity = 0.166
F_{ij}	Configuration factor: percent of radiation leaving diffuse surface i that strikes surface j
I	Intensity (w/cm^2-sr-μm)
K	Detector constant, v/w
K′	Detection constant dependent on both detector and detection optics, v/w
L	Blackbody depth, cm
ℓ	Length, in.
$\dot{Q}$	Power, w
$\dot{q}$	Power per unit area
u	Detector output due to nonvarying emission of components, v
v	Detector output due to component emission, v
α	Angle, deg
β	Radiance polar angle, deg
γ	Radiance azimuthal angle, deg
δ	Angle, deg
ϵ	Emissivity
ζ	Irradiance azimuthal angle, deg
θ	Polar angle of reflected radiation from test surface, deg
λ	Wavelength, μm
μm	Micrometers

ρ	Reflectance, percent
σ	RMS surface roughness, μm
τ	Transmission
ϕ	Azimuthal angle of reflected radiation from test surface, deg
ψ	Irradiance polar angle, deg
ω	Solid angle

SUBSCRIPTS

b	Blackbody
bd	Bidirectional
c	Chopper
hd	Hemispherical-directional
i	Incident
M	Mirror
R	Reflected
Ref	Reference surface
S	Sample
TO	Transfer optics